

REF ID: A220 839

2

AD-A220 839

NSWC TR 89-99

# NONAXISYMMETRIC BODY, SUPERSONIC, INVISCID DYNAMIC DERIVATIVE PREDICTION

BY LEROY DEVAN  
WEAPONS SYSTEMS DEPARTMENT

JUNE 1989

Approved for public release; distribution is unlimited.

DESTRUCTION NOTICE -- For classified documents, follow the procedures in DOD 5220 22M, Industrial Security Manual, Section II-19, or OPNAVINST 5510.1H, Chapter 17. For unclassified, limited documents, destroy by any method that will prevent disclosure of contents or reconstruction of the document.

DTIC  
ELECTE  
APR 23 1990  
S E D  
to



**NAVAL SURFACE WARFARE CENTER**  
Dahlgren, Virginia 22448-5000 • Silver Spring, Maryland 20903-5000

000

**REPORT DOCUMENTATION PAGE**

1 OFFICIAL USE ONLY		2 REPORT DATE June 1989	3 TYPE OF REPORT AND DATES COVERED Final	
4 TITLE AND SUBTITLE Nonaxisymmetric Body, Supersonic, Inviscid Dynamic Derivative Prediction			5 FUNDING NUMBERS Project Numbers: RA11G13 RU11G14 RU11811	
6 AUTHOR(S) Leroy Devan				
7 PERFORMING ORGANIZATION NAME(S) AND ADDRESS(ES) Naval Surface Warfare Center (G23) Dahlgren, VA 22448-5000			8 PERFORMING ORGANIZATION REPORT NUMBER	
9 SPONSORING/MONITORING AGENCY NAME(S) AND ADDRESS(ES)			10 SPONSORING/MONITORING AGENCY REPORT NUMBER NSWC TR 89-99	
11 SUPPLEMENTARY NOTES				
12a DISTRIBUTION AVAILABILITY STATEMENT Approved for public release; distribution is unlimited.			12b DISTRIBUTION STATEMENT CODE	
13 ABSTRACT (MAXIMUM 200 WORDS) <p>A supersonic, aerodynamic computational model, which is the basis of the NANC code, has been extended to compute dynamic derivatives. The extension is to the inviscid contribution of constant angular rates and axial accelerations.</p> <p>The body geometry limitations are the same as for the steady-state model. Here, a pointed body or equivalent pointed body is assumed for low Mach numbers; at higher Mach numbers, the effect of axial acceleration is neglected and the body may be blunt. The body may be noncircular with planar discontinuities, including inlets, with fins (up to six per fin set), which lie on a cylindrical coordinate ray.</p> <p>For the low Mach number range, the original second-order potential model has been extended for angular rate derivative prediction. For the acceleration rate derivatives, a "hybrid" first- and second-order model has been developed.</p> <p>For the high Mach number range, an equivalent angle-of-attack vector is defined and combined with local solution models.</p> <p>Computational comparisons are made with experimental data, primarily for pitch and roll damping derivatives.</p>				
14 SUBJECT TERMS Dynamic derivatives; supersonic, aerodynamic computational model; first- and second-order model; roll, pitch damping; fin Magnus			15 NUMBER OF PAGES 50	
			16 PRICE CODE	
17a SECURITY CLASSIFICATION (OF REPORT) UNCLASSIFIED	17b SECURITY CLASSIFICATION (OF PAGE) UNCLASSIFIED	17c SECURITY CLASSIFICATION (OF ABSTRACT) UNCLASSIFIED	18 NAME OF TYPE	

**FOREWORD**

This work represents an extension of the work reported in Naval Surface Warfare Center (NSWC) TR 86-253. The latter report presented computational methods for predicting aerodynamic loading for supersonic Mach numbers on non-axisymmetric flight vehicles at constant or steady incidence. The extension is for the prediction of aerodynamic loading or dynamic derivatives associated with constant body axis angular rates and/or acceleration. The resulting computer program allows one to predict roll and pitch damping, fin Magnus, and other dynamic derivatives for the preliminary and intermediate design stage.

Support for the work was provided by the following sponsors:

1. Aerodynamics and Structures Block of the Surface-Launched Weaponry Technology Program Project Numbers RA11G13/RU11G14.
2. Air-Launched Antisurface Weaponry Technology Project Number RU11811.

This report was reviewed and approved by Dr. T. J. Rice, Head, Aeromechanics Branch and C. A. Cooper, Head, Missile Systems Division.

Accession For	
NTIS GFA&I	<input checked="" type="checkbox"/>
DTIC TAB	<input type="checkbox"/>
Unannounced	<input type="checkbox"/>
Justification	
By	
Distribution/	
Availability Codes	
Dist	Avail and/or Special
A-1	

Approved by:

*J. L. Sloop*  
 J. L. SLOOP, Deputy Head  
 Weapons Systems Department

## CONTENTS

<u>Section</u>		<u>Page</u>
1.0	INTRODUCTION . . . . .	1
2.0	GEOMETRY, FREE-STREAM VELOCITY AND FORCE CONVENTIONS . . . . .	2
3.0	THEORETICAL DEVELOPMENT . . . . .	3
	3.1 FIRST- AND SECOND-ORDER POTENTIAL EQUATIONS . . . . .	3
	3.2 COMPUTATIONAL COORDINATES AND GRIDS . . . . .	6
	3.3 NUMERICAL METHODS . . . . .	6
	3.4 LOADING COEFFICIENTS AND OTHER NUMERICAL CONSIDERATIONS . . . . .	8
	3.5 HIGH MACH NUMBER SOLUTION . . . . .	9
4.0	EVALUATION OF THE NUMERICAL METHODS . . . . .	9
	4.1 BODY-ALONE COMPARISONS . . . . .	10
	4.2 BODY-TAIL CONFIGURATIONS . . . . .	10
	4.3 BODY-WING-TAIL OR BODY-CANARD-TAIL CONFIGURATIONS . . . . .	12
5.0	CONCLUDING REMARKS . . . . .	13
6.0	REFERENCES . . . . .	13
	APPENDIX: NOMENCLATURE . . . . .	A-1
	DISTRIBUTION . . . . .	(1)

## ILLUSTRATIONS

<u>Figure</u>		<u>Page</u>
1	HALF BODY GEOMETRY . . . . .	16
2	THIN FIN GEOMETRY . . . . .	16
3	FIN PLANFORM GEOMETRY . . . . .	17

## ILLUSTRATIONS (CONTINUED)

<u>Figure</u>		<u>Page</u>
4	$C_{mq'} + C_{m\dot{\alpha}}$ COMPARISONS FOR A CIRCULAR CONE, $L_N = 2.98$ CALIBERS, $x' = 2.18$ FROM NOSE. . . . .	. 17
5	$C_{mq'} + C_{m\dot{\alpha}}$ FOR A CONE-CYLINDER, $L_N = 2.98$ CALIBERS, $L = 5.12$ CALIBERS, $x' = 3.44$ CALIBERS FROM NOSE . . . . .	. 18
6	$C_{mq'} + C_{m\dot{\alpha}}$ COMPARISON FOR THE ARMY-NAVY SPINNER, $L_N = 2.0$ CALIBERS, $L = 5.0$ CALIBERS, $x' = 3.0$ CALIBERS FROM NOSE . . . . .	. 18
7	$C_{mq'} + C_{m\dot{\alpha}}$ FOR THE ARMY-NAVY SPINNER, $L_N = 2.0$ CALIBERS, $L = 9.0$ CALIBERS, $x' = 5.06$ CALIBERS FROM NOSE . . . . .	. 19
8	$C_{Nq'} + C_{N\dot{\alpha}}$ COMPARISON FOR AN ELLIPTIC CONE . . . . .	. 19
9	$C_{mq'} + C_{m\dot{\alpha}}$ COMPARISON FOR AN ELLIPTIC CONE . . . . .	. 20
10	BASIC FINNER CONFIGURATION . . . . .	. 20
11	BASIC FINNER $C_{lp'}$ COMPARISON . . . . .	. 21
12	$C_{np'\dot{\alpha}}$ , MAGNUS DERIVATIVE FOR THE BASIC FINNER . . . . .	. 21
13	TOTAL PITCH DAMPING COMPARISON FOR THE BASIC FINNER . . . . .	. 22
14	ASPECT RATIO = 3 CONFIGURATIONS . . . . .	. 22
15	PITCH DAMPING COMPARISON FOR AN AR = 3 WING- BODY CONFIGURATION . . . . .	. 23
16	AIR SLEW DEMONSTRATOR VEHICLE. . . . .	. 23
17	PITCH DAMPING COMPARISON FOR THE AIR SLEW DEMONSTRATOR VEHICLE . . . . .	. 24
18	XM-144 CONFIGURATION . . . . .	. 24
19	TOTAL PITCH DAMPING FOR THE XM-144 . . . . .	. 25
20	BRL M735 CONFIGURATION . . . . .	. 25
21	ROLL DAMPING COMPARISON COMPUTATIONS FOR THE M735 PROJECTILE . . . . .	. 26

## ILLUSTRATIONS (CONTINUED)

<u>Figure</u>		<u>Page</u>
22	TOTAL PITCH DAMPING COMPARISON FOR THE M735 PROJECTILE . . . . .	26
23	SIDEWINDER GEOMETRY . . . . .	27
24	TOTAL PITCH DAMPING COMPARISON FOR THE SIDEWINDER . . . . .	27
25	TOTAL PITCH DAMPING COMPARISON FOR THE RFL 122 . . . . .	28
26	TOTAL PITCH DAMPING COMPARISON FOR AN AEROSPATIALE MISSILE CONFIGURATION . . . . .	28

## 1.0 INTRODUCTION

Preliminary design requires the estimate of aerodynamics for a large set of free-stream and geometric variations. To keep computational costs reasonable, rapid (but reasonably accurate) methods are sought and utilized.

For cruciform finned, axisymmetric bodies at low angle of attack, component buildup methods<sup>1,2</sup> can be utilized for a restricted range of configurations and free-stream conditions that are applicable to current designs.

Linear surface singularity methods<sup>3,4</sup> have been highly developed for complex configurations, including high angle-of-attack vortex modelling. Set-up and run times are fairly long.

The second-order Van Dyke model<sup>5</sup>, which corrects for compressibility effects, was extensively modified and adapted for noncircular bodies with planar discontinuities, including inlets, and multi-sets of fins.<sup>6-9</sup> The NANC code<sup>10-12</sup> includes the second-order potential model plus a local solution model based on the methods of Reference 13.

Dynamic derivative estimates are calculated in the NSWC Aeroprediction code of Reference 1. Body-alone contributions are given by an empirical data fit. Fin-alone contributions are given by thin-wing theory. Interference modelling is incomplete when compared with the static case. Thin-wing theory is based on conical solutions that are not valid for small aspect ratio fins.

Dynamic derivative estimation is primarily of interest for unguided applications. Pitch damping is usually ignored for guided applications since the autopilot provides control surface moments, which are proportional to the pitch rate and significantly larger.

Classical unsteady aerodynamics is based upon the unsteady linear potential equation.<sup>14</sup> The unsteady potential equation may be applied to harmonic analysis of the rigid motion or to aeroelastic applications. The harmonic gradient method of Reference 15 is a singularity collocation code utilizing a complex potential. The total pitch damping for low frequency is the same as for the constant pitch and acceleration rate estimate.

The NANC code is modified in this report to compute forces and moments which are a function of constant axial rotation rates and moment center accelerations. The remainder of the report assumes that the reader is familiar with the

earlier work summarized in Reference 10 and concentrates on the dynamic derivative modifications.

## 2.0 GEOMETRY, FREE-STREAM VELOCITY AND FORCE CONVENTIONS

Assumptions concerning body and fin geometry are the same as in Reference 10. Figures 1 through 3 are taken from Reference 10. However, the body is assumed to have a pointed nose for the low Mach number range.

A static blunt body model establishes a matching plane of velocity component data by matching a modified Newtonian pressure distribution and utilizing conical potential functions and other assumptions. A blunt body model for the plunging acceleration problem was not deemed feasible. A model for pure axial rotation is only somewhat more feasible.

Computations utilize a cylindrical coordinate system and the "thin-fin" approximation with the fin midplane lying on a cylindrical coordinate ray. The body is divided into sections by planar discontinuities (including planar inlets). Any section except the first may have a set of fins with up to six fins. See Reference 10 for a more detailed discussion.

Force convention is the same as used in earlier work. The axial force,  $F_A$ , acts in the x direction; the normal force,  $F_N$ , acts in the z direction; and the side force,  $F_Y$ , acts in the negative y direction. The roll moment,  $M_\ell$ , acts in the negative x direction; the yawing moment,  $M_n$ , acts in the negative z direction; and the pitching moment,  $M_m$ , acts in the negative y direction.

The main difference between the current work and earlier work is the body-axis oriented equivalent dimensionless free-stream velocity vector. In Cartesian coordinates, the velocity vector relative to body axes, in dimensionless form, is given as

$$\begin{aligned}
 q_{0x} &= \left[ \frac{\dot{u}_0 t}{V_r} + \frac{-q'z + r'y}{V_x} + \cos\alpha \cos\beta' \right] i' \\
 &+ \left[ \frac{\dot{v}_0 t}{V_x} + \frac{-r'(x - x') + p'z}{V_x} + \sin\beta' \right] j' \\
 &+ \left[ \frac{\dot{w}_0 t}{V_r} + \frac{p'y + q'(x - x')}{V_r} + \sin\alpha \cos\beta' \right] k' \\
 &= q_r + \dot{q}_r t \quad \lim t \rightarrow 0
 \end{aligned} \tag{2-1}$$

Note that the time derivatives of the axial rotation rates could be included as well, but are neglected.  $p'$ ,  $q'$ ,  $r'$  are the axial rotation rates in the negative  $x$ ,  $y$ , and  $z$  directions, respectively, and  $\dot{u}_0$ ,  $\dot{v}_0$ , and  $\dot{w}_0$  are the corresponding acceleration rates. For the total pitch damping problem,  $q'$  and  $\dot{w}_0$  are the pertinent input terms.  $\alpha$  and  $\beta'$  are the angle of attack and side slip, respectively.

An additional symmetry operation variation for LM (defined in Reference 10) is introduced here. LM = 1 is for axial force as the only nonzero force term. LM = 2 is for axial force and rolling moment as the only nonzero forces. The new symmetry value for LM = 2 is for a circular body with quarter-plane symmetric fin distribution and a roll control deflection or constant roll rate. For the LM = 2 case, the computation is LM = 1 before the first fin set and LM = 2 subsequently. LM = 3 is for the axial force, normal force, and pitching moment nonzero. LM = 5 is for axial force, side force, and side moment nonzero. LM = 6 is for a full plane computation. LM is defined for each section of the body and must increase or remain the same as the computation is marched down the body.

### 3.0 THEORETICAL DEVELOPMENT

#### 3.1 FIRST- AND SECOND-ORDER POTENTIAL EQUATIONS

The full nonlinear, dimensionless, potential equation is

$$a^2 \nabla \cdot \mathbf{Q} = M_r^2 \left[ \frac{1}{V_r^2} \frac{\partial^2 \phi}{\partial t^2} + \frac{1}{V_r} \frac{\partial \mathbf{Q}^2}{\partial t} + \frac{\mathbf{Q} \cdot \nabla \mathbf{Q}^2}{2} \right] \quad (3-1)$$

Here,  $a$  is the speed of sound divided by  $a_r$  and  $\mathbf{Q} = \nabla \phi$  is the dimensionless velocity vector. Equation (3-1) is appropriate to a body moving through a fluid at rest. It is derived from the continuity equation, momentum equations, and the Bernoulli relationship. For body-fixed coordinates,

$$\frac{\partial}{\partial t} = \frac{\partial}{\partial t} - \mathbf{V} \cdot \nabla \quad (3-2)$$

$$\mathbf{V} = -\mathbf{q}_{0\infty} \quad (3-3)$$

In addition, the relative velocity,  $\mathbf{q}_r = \mathbf{Q} - \mathbf{V}$ , is introduced. The continuity equation then becomes

$$\frac{1}{V_r} \frac{1}{\rho} \frac{\partial \rho}{\partial t} + \nabla \cdot \mathbf{q}_r + \frac{1}{\rho} (\mathbf{q}_r \cdot \nabla) \rho = 0 \quad (3-4)$$

The Bernoulli relationship for body coordinates becomes

$$M_r^2 \left[ \frac{1}{V_x} \frac{\partial \phi}{\partial t} + \frac{q_r^2 - V^2}{2} \right] + \frac{a^2}{\gamma - 1} = \frac{1}{\gamma - 1} \quad (3-5)$$

The density may be eliminated from Equation (3-4) by using Equation (3-5) to yield

$$a^2 \nabla \cdot q_r = M_r^2 \left[ q_r \cdot \nabla \left( \frac{q_r^2 - V^2}{2} \right) + \frac{1}{V_x^2} \frac{\partial^2 \phi}{\partial t^2} + \frac{\partial}{\partial t} \left( \frac{q_r^2 - V^2}{2} \right) + q_r \cdot \frac{\partial q}{\partial t} \right] \quad (3-6)$$

$$a^2 = 1 + \frac{\gamma - 1}{2} M_r^2 \left[ V^2 - q_r^2 - \frac{2 \left( \frac{\partial \phi}{\partial t} \right)}{V_x} \right] \quad (3-7)$$

A small disturbance from the static free-stream dimensionless velocity vector is given by

$$q_r = i' + (q_{0x} - i') + q = i' + q'_x + q \quad (3-8)$$

Substitution of Equation (3-8) into Equation (3-6) and neglecting higher order terms yields the first-order wave equation

$$\nabla \cdot q'_1 = M_x^2 \left[ \frac{1}{V_x^2} \frac{\partial^2 \phi'_1}{\partial t^2} + 2 \left( \frac{\partial u'_1}{\partial t} \right) + \frac{\partial^2 \phi_1}{\partial x^2} \right] \quad (3-9)$$

$q'_1$  is the first-order velocity vector,  $u'_1$  the x component of  $q'_1$ , and  $\phi'_1$  the corresponding potential function.

The first-order problem may be further broken down into three steady problems.

$$\phi'_1 = \phi_1 + \frac{M_x^2}{\beta^2} \phi_a + V_x \left[ t - \frac{x M_x^2}{\beta^2 V_x} \right] \phi_b \quad (3-10)$$

Here  $\phi_1$  is the potential function associated with the angle-of-attack problem and axial rotation rates.  $\phi_a$  and  $\phi_b$  are equivalent steady potential functions associated with the plunging rate problem. Equation (3-10) satisfies Equation (3-9) when  $\phi_1$ ,  $\phi_a$ , and  $\phi_b$  satisfy the steady first-order wave equations

$$(\nabla \cdot q_\ell)_c - \beta^2 \frac{\partial u_\ell}{\partial x} = 0 \quad (3-11)$$

$$(\nabla \times q_\ell)_c = 0 \quad (3-12)$$

$\ell = 1, a, b; c$  stands for the crossflow plane and components.

As in earlier work, an improved solution to the first-order problem is obtained by evaluating the neglected nonlinear terms using the first-order solution and solving a nonhomogeneous potential equation. Only time-independent terms are considered.

$$(\nabla \cdot q_2)_c - \beta^2 \frac{\partial u_2}{\partial x} = M_x^2 \nabla \cdot \Omega \quad (3-13)$$

$$(\nabla \times q_2)_c = 0 \quad (3-14)$$

$$\Omega = \Omega_{x'} + \Omega_c \quad (3-15)$$

$$\begin{aligned} \Omega_x = u_1 \left[ \frac{1}{2} q_1^2 - \frac{(2-\gamma)}{6} M_x^4 u_1^2 - \frac{(2-\gamma)}{2} M_x^2 q_{1c}^2 - 1 \right] \\ + u_x \left[ \frac{\gamma-1}{2} M_x^2 u_1^2 + q_1^2 + q_x \cdot q_1 \right] \end{aligned} \quad (3-16)$$

$$\begin{aligned} \Omega_c = q_{1c} \left[ \frac{q_1^2}{2} + \frac{2-\gamma}{2} M_x^2 u_1^2 \right] + q_{xc} (q_1^2 + q_x \cdot q_1) \\ + \frac{M_x^2}{\beta^2} (\gamma-1) \left[ \frac{q_{1c}^2}{2} q_{xc} + q_{1c} \times (q_{1c} \times q_{xc}) \right] \end{aligned} \quad (3-17)$$

Boundary conditions for first- and second-order problems are

$$(q_\ell + q_x) \cdot n = 0 \quad (3-18)$$

$\ell = 1, 2$

The equivalent steady problem boundary conditions for the  $\dot{q}_x$  problems are

$$\left( q_b + \frac{\dot{q}_x}{V_x} \right) \cdot n = 0 \quad (3-19)$$

$$\left( q_a + x \frac{\dot{q}_x}{V_x} \right) \cdot n = - \frac{\partial r_b}{\partial x} \Phi_b \quad \text{body} \quad (3-20)$$

$$\left( q_a + x \frac{\dot{q}_x}{V_x} \right) \cdot n = -t_x \Phi_b \quad \text{fin}$$

Here,  $\partial r_b / \partial x$  and  $t_x$  are body and fin slopes, respectively.

### 3.2 COMPUTATIONAL COORDINATES AND GRIDS

The region between the body and the Mach cone is mapped to the rectangular region shown in Figure 2 by the shearing transformation

$$\xi = \frac{r - r_b}{x/\beta - r_b} \quad (3-21)$$

Further clustering transformations  $\xi = \xi(\zeta)$  and  $\Phi = \Phi(\theta)$  are used for nonuniform gridding of the  $\theta$  and  $\xi$  variables. The functional dependencies are not given explicitly. See Section 3.2 in Reference 10 for more details.

### 3.3 NUMERICAL METHODS

Most of the numerical methods are as reported in Reference 10. However, some of them have been changed.

The implicit formulation for the first body section is as in earlier work. The velocity vector advancement Equations (3-11) through (3-14) are single second-order equations in a potential,  $\phi = xF$ .<sup>6,7</sup>  $F$  is known as a conical potential function. However, actual conical similarity for the total pitch damping problem requires the functional form of  $\phi = x(G + xH)$ . The pressure distribution on a cone is now linear with  $x$  instead of constant. Therefore, the computation uses more than two steps for a solution for a cone. The solution at  $x = 0$  is assumed to be conical. However, the resultant computation for a numerical solution using a few marching steps does not vary significantly from a solution developed based on the true conical similarity of  $\phi = x(G + xH)$  and two marching steps.

At body planar discontinuities and supersonic leading and trailing edges, the jump in various velocity components is obtained by application of the method of "weak solutions"<sup>16</sup> combined with a downstream boundary condition and conservation of the velocity component tangent to the discontinuity edge condition. At a subsonic leading edge, the solution for the velocity jumps does not exist and the conservation relationship provided by the method of "weak solutions" must be replaced by a heuristic one. The "weak solution" conservation relation is modified due to the modified Equation (3-13).

For all sections, except the first, the conservation velocity vector advancement equations are solved using a MacCormack<sup>17</sup> predictor-corrector scheme for points not on a solid surface. Body and fin surface velocities are advanced by characteristic compatibility relations (two in number) combined with a solid surface boundary

condition.<sup>18</sup> At a corner where the fin and body meet, no unique solution is possible. The advancement equations for the fin-body junction have been modified. The fin-body junction line is assumed to be a streamline. Therefore, fin and body boundary conditions and one other condition are needed to solve for the three velocity components.

One estimate of the axial velocity component,  $u$ , can be obtained from one body advancement quantity and the body boundary condition.

$$E_B = u_B \beta \sqrt{1 + \epsilon_\theta^2} + v_B - \epsilon_\theta w_B \quad (3-22)$$

$$v_B - \epsilon_\theta w_B = \frac{\partial Y_b}{\partial x} (u_B + u'_x) - v'_x + \epsilon_\theta w'_x \quad (3-23)$$

Here,  $u$ ,  $v$ , and  $w$  are the axial, radial, and  $\theta$  components of velocity.  $\epsilon_\theta = 1/r_b(\partial r_b/\partial \theta)$ . The B subscript stands for the body. For the first- and second-order problem,  $u'_x$ ,  $v'_x$ , and  $w'_x$  are free-stream velocity components. For the  $\phi_b$  problem,  $q'_x = \dot{q}_x$ . For the  $\phi_a$  problem,  $u'_x = \dot{u}_x x/V_x - \phi_b$ ,  $v'_x = \dot{v}_x x/V_x$ , and  $w'_x = \dot{w}_x x/V_x$ .  $u_B$  is obtained from Equations (3-22) and (3-23).  $E_B$  is known.

A second estimate of the axial velocity component is obtained from the fin advancement quantity and the fin boundary condition

$$E_F = \pm \beta u_F + w_F \quad (3-24)$$

$$w_F = -w'_x + t_x (u_F + u'_x) \quad (3-25)$$

Here,  $E_F$  is known.  $u_F$  may be obtained from Equations (3-24) and (3-25). The upper sign is for the  $\theta > \theta_{fin}$  side of the fin.

The final values of  $u$ ,  $v$ ,  $w$  for the fin-body junction are obtained from

$$u = \frac{1}{2} (u_B + u_F) \quad (3-26)$$

$$v - \epsilon w = \frac{\partial r_b}{\partial x} (u + u'_x) - v'_x + \epsilon_\theta w'_x \quad (3-27)$$

$$w = -w'_x + t_x (u + u'_x) \quad (3-28)$$

Note that  $\phi_b$  need only be determined on the solid surfaces and is needed for the  $\phi_a$  problem boundary condition and evaluation of the Bernoulli pressure coefficient relationship. An advancement equation for  $\phi_b$  is given by

$$\frac{d\phi_b}{dx} = u_b + \left[ \frac{\partial r_b}{\partial x} (1 - \xi) + \frac{\xi}{\beta} \right] v_b + t_x w_b \quad (3-29)$$

On a body surface or interior point,  $t_x$  is set to zero.

A subsonic leading edge requires a modification of the jump relations. For all cases,

$$u_{k,j} = u_{k-1,j} \sqrt{r_0^2 - r_{k-1,j}^2} / \sqrt{r_0^2 - r_{k,j}^2} \quad (3-30)$$

$k$  is the grid index in the  $r$  direction;  $j$  is the index in the  $\theta$  direction. Equation (3-30) combined with downstream boundary condition and conservation of the velocity component tangent to the edge provides a solution for the downstream values of velocity. The square root ratio is limited to a value of 2.  $r_0$  is the radius of the leading edge. Equation (3-30) has the well known square root singularity for a subsonic leading edge.

### 3.4 LOADING COEFFICIENTS AND OTHER NUMERICAL CONSIDERATIONS

The axial acceleration rates contribution to velocities in the limit as  $t \rightarrow 0$  is given by differentiation of the last two terms of Equation (3-10).

$$q_{ax} = \frac{M_\infty^2}{\beta^2} \left[ q_a - x q_b \right] - i' \frac{M_r^2}{\beta^2} \Phi_b \quad (3-31)$$

The first- or second-order pressure coefficient is then given by

$$C_p = (\chi^{3.5} - 1) / (.7 M_\infty^2) \quad (3-32)$$

$$\chi = 1 + .2 M_\infty^2 (q_a^2 - Q_{T\ell}^2 - 2\Phi_b) \quad (3-33)$$

$$Q_{T\ell} = q_{ax} + q_r + q_\ell \quad \ell = 1, 2 \quad (3-34)$$

This is a "hybrid" model for the plunging rate case since  $q_{ax}$  is a first-order potential quantity.

The inviscid loading coefficients are as given in Section 5.0 of Reference 10.

Smoothing of the MacCormack vector quantities is an input option for sections with fins. It is particularly needed for subsonic leading edges.  $Q_{T1}^2$  with  $q_{ax} = 0$  is used as a weighting function for first- and second-order vector terms as in Section 3.11 of Reference 10.  $Q_{T1}^2$  with  $q_{ax} \neq 0$  is used as a weighting function for the  $\phi_a$  and  $\phi_b$  problem vector terms.

The explicit marching solution will fail when  $x$  becomes negative in Equation (3-32). For  $\dot{q}_x = 0$ ,  $x$  is set to zero or the vacuum value and the velocities are adjusted as discussed in Section 3.11 of Reference 10. For  $\dot{q}_x \neq 0$  and  $x$  negative, the solution is halted and an error message is written to the output file.

### 3.5 HIGH MACH NUMBER SOLUTION

The potential model breaks down at Mach numbers where the origin Mach cone crosses the body surface.  $\dot{q}_x$  is set to zero for this local solution model.

The velocity vector,  $q_x$ , is normalized to 1 as

$$q'_x = q_x / |q_x| \quad (3-35)$$

$q'_x$  is then used to find the turning angle between an effective free-stream velocity vector and the local surface normal. These are combined with the local solution methods of Reference 13. It is expected that these local solution methods will be inaccurate below  $M_x = 4$ . Note that blunt bodies may be considered.

### 4.0 EVALUATION OF THE NUMERICAL METHODS

Evaluation is almost exclusively made by comparison with experimental data. The data sources are ballistic range data or wind tunnel tests. Dynamic derivatives must be based on parameter estimation techniques associated with kinematic data and an assumed aerodynamic model. In general, the accuracy and repeatability of the estimated coefficients is much worse than for static coefficients.

The code development is for nonaxisymmetric bodies with combined angle of attack, control deflection, rotation rates, and axial accelerations. Data, however, is mostly available for  $C_{lp}$  and  $C_{mq} + C_{m\dot{\alpha}}$  for circular bodies at zero incidence. Computations are separate for  $C_{lp}$ ,  $C_{mq}$ , and  $C_{m\dot{\alpha}}$ .

The dynamic derivatives are given in general form as

$$C_i = \frac{M_i}{S_R x_R Q_D (\omega_i x_D / V_\infty)} \quad (4-1)$$

$S_R$  is a reference area;  $x_R$  is a reference length;  $M_i$  is a force or moment;  $Q_D$  is the dynamic pressure;  $x_D$  is a length associated with a reduced frequency; and  $\omega_i$  is an axial roll rate or dimensionless acceleration.

#### 4.1 BODY-ALONE COMPARISONS

The reference area for bodies will be the maximum cross-sectional area.

The first computation is for a 2.98 caliber length cone. The moment center is located 2.18 calibers from the nose.  $x_R$  is the maximum body diameter and  $x_D$  is the maximum body radius. Unless otherwise indicated, references will not vary in the rest of the report. Figure 4 compares  $C_{mq'} + C_{m\dot{\alpha}}$  computational values with values extracted from the ballistic range data of Reference 19. The usual lack of repeatability of the data is shown due to different initial yaws and, hence, epicyclic history. Figure 5 compares  $C_{mq'} + C_{m\dot{\alpha}}$  computational values for a cone-cylinder and the ballistic range data of Reference 19.

The next comparison computations are for the Army-Navy Spinner configurations. These configurations have 2-caliber secant ogive noses with arc radii twice that of a tangent ogive and various body lengths and moment center locations. Figure 6 compares  $C_{mq'} + C_{m\dot{\alpha}}$  computations with data for a 5-caliber length body. Note the great differences between different range tests and wind tunnel tests. Also plotted are  $C_{m\dot{\alpha}}$  and a slender body value. Figure 7 compares  $C_{mq'} + C_{m\dot{\alpha}}$  computations with data for a 9-caliber length body. GE-Spinner refers to the empirical curve fit of Reference 20.

The final body computational example is taken from Reference 15.  $x_R$  and  $x_D$  are cone lengths,  $L$ , for an elliptic cone. Semi-minor to semi-major axis ratio is  $a/b = .75$ .  $a/L = .0866$ ,  $x' = 0$ . Figure 8 compares  $C_{Nq'} + C_{N\dot{\alpha}}$  first- and second-order computations with that of Reference 15. Figure 9 compares  $C_{mq'} + C_{m\dot{\alpha}}$ . Computations for  $C_{N\dot{\alpha}}$  show significant differences between first- and second-order order. The computation of Reference 15 is a first-order computation using different numerical methods. Three computational planes seems to be adequate for this case.

#### 4.2 BODY-TAIL CONFIGURATIONS

The first configuration considered for this section is the Basic Finner of Figure 10.21,22 Figure 11 shows a comparison of data with computation for the roll damping derivative. The loading for the roll damping problem is low near the body and increases with span distance. The roll moment loading increases even more rapidly with span distance. At a side edge, the loading drops to zero. Load integration routines were modified to try to account for the sharp drop off of loading near a side edge. This improved  $C_{lp'}$  prediction at lower Mach numbers. Figure 12 depicts a Magnus moment derivative,  $C_{Np'\dot{\alpha}}$ , computation comparison with data. A body-alone estimate using the empirical computation of Reference 20 indicates a variation of -.4 to 3 for the Mach number range of 1.2 to 3. The computation here only follows for the data trend but not the magnitude. Figure 13 depicts a total pitch damping comparison. A trend of being above the data at lower Mach numbers is indicated here.

The next configuration is that of Figure 14(b) taken from Reference 23. The equation of the body in calibers is

$$\begin{aligned} r_b &= .5|1 - (1 - x/6.25)^2|^{3/4} & 0 < x < 6.25 \\ r_b &= .5, x > 6.25 \end{aligned} \quad (4-2)$$

Since  $\partial r_b/\partial x$  and  $\partial^2 r_b/\partial x^2$  are singular at  $x = 0$ , the nose is approximated as

$$r_b = .29716844x - .131673491x^2 + .034340881x^3 \quad 0 < x < 1 \quad (4-3)$$

Equation (4-3) matches zero through second derivatives of Equation (4-2) at  $x = 1$ . The total pitch damping comparison is shown in Figure 15. Reference area is the extended to centerline fin planform area (two fins). Reference  $x_R = 2x_D =$  the mean aerodynamic chord,

$$C' = \frac{2}{3} \frac{(C_r^2 + C_t^2 + C_t C_r)}{C_t + C_r} \quad (4-4)$$

Here,  $C_r$  and  $C_t$  are root and tip chords of the extended fin. The moment center is  $.2C'$  from the apex of the wing extended to the body centerline. Leading and trailing edges are supersonic and the computation compares fairly well with the data. Computations were adequate for the configuration of Figure 14(a) for supersonic leading edges, but very poor for subsonic edges when the moment center is  $.35C'$  from the extended wing apex. The reason is the inaccurate computation of  $C_{m\dot{\alpha}}$ . For moment centers which are, more typically, not close to the point of action of  $C_N\dot{\alpha}$ , the sensitivity and accuracy is better.

The next configuration considered is depicted in Figure 16. A  $C_{mq}' + C_{m\dot{\alpha}}$  comparison for this configuration is shown in Figure 17. Here, the trend of over-prediction is reversed.

The next body-tail configuration considered is the flechette of Figure 18 taken from Reference 24. Reference 24 (unpublished) compares one of the routines for computing total pitch damping in Reference 1 with available data for a large number of body-alone and body-tail configurations. The XM-144 body end radius of .005 calibers is approximated as .05 calibers. Figure 19 compares computations with data. For this case, the leading edge of the fins is subsonic below Mach numbers of 3.25. The data was surprisingly smooth for this configuration. The boat tail has a significant effect on the computational results.

The final body-tail configuration<sup>25</sup> of Figure 20 has six fins and a boat-tail angle of 2 deg. Figure 21 compares  $C_{lp}'$  potential and local computations with the PNS computations of Reference 25. The sharp rise close to sonic leading edge conditions is predicted by the thin-fin, fin-alone methods of Reference 1. The boat tail

significantly affects the solution. Figure 22 shows a pitch damping computational comparison with data for a configuration close to that of Figure 20. The configuration and data are from Reference 24. Here, the conical nose length is 3.32 calibers and the moment center is 7.14 calibers from the nose. From Figures 21 and 22, one can see that the local solution is of limited value.

#### 4.3 BODY-WING-TAIL OR BODY-CANARD-TAIL CONFIGURATIONS

Here, the additional interference of forward lifting surfaces on the tail is the primary phenomenon. As in earlier work, it is assumed that the velocity vector downstream of a supersonic trailing edge lies on a constant cylindrical ray plane,  $\theta = \theta_f$ .

The first computational comparison is for the B-C-T configuration of Figure 23. Figure 24 shows a computational comparison with experimental data. The trend at lower Mach numbers is as noted earlier. Here, the carryover canard to tail of  $C_{m\dot{\alpha}}$  grows as the Mach number decreases. Evaluation of the plunging acceleration contribution of Equation (3-31) involves  $M_\infty^2/\beta^2$  and differences which probably become sensitive as the Mach number is decreased. Computations of  $C_{lp'}$  also indicate a carryover effect which is not accounted for by component superposition methods. At  $M_\infty = 1.76$ ,  $C_{lp'} = -199.3$  for the total configuration. For the same Mach number, the total of individual canard and tail configurations adds up to  $C_{lp'} = -171.1$ .

Figure 25 compares total pitch damping with data and a semi-empirical estimate for the RFL 122 configuration of Reference 26. The ordinate scale was not given and is inferred here. The  $C_{m\dot{\alpha}}$  carryover phenomenon seems to be less extreme in this case. The semi-empirical estimate seems to be worse, assuming the data fit is correct. A  $C_{lp'}$  computation at  $M_\infty = 1.5$  yields -89.5 for the total configuration. The wing contribution to  $C_{lp'}$  at the same Mach number is -94.0.

The final computation is for the B-W-T configuration of Reference 27. Total pitch damping comparison and configuration are depicted in Figure 26. Geometry and the moment center location are given in Reference 27. The geometry was scaled from Reference 27.  $x'$  is assumed to be at  $x' = 8.5$  calibers from the nose. The  $C_{m\dot{\alpha}}$  carryover phenomenon is noted as before. Missile refers to an Aerospatiale semi-empirical code.

## 5.0 CONCLUDING REMARKS

The computational methods, developed for computing static aerodynamic coefficients for noncircular bodies at supersonic Mach numbers, have been extended to the computation of dynamic derivatives.

Geometric limitations are the same as for the earlier work. However, it is assumed that the bodies are pointed.

The weakest elements in the original code are exaggerated here since moments are almost exclusively computed. The variation of pressures close to subsonic leading and side edges is affected by edge singularities.  $C_{lp}$  prediction is poorest for fins with low aspect ratios.  $C_{mq} + C_{m\dot{\alpha}}$  prediction is poorest when the leading edge is subsonic and the point of action of  $C_{Nq} + C_{N\dot{\alpha}}$  is close to the moment center. The carryover effect for  $C_{m\dot{\alpha}}$  is overpredicted when the leading edges are subsonic for bodies with two sets of lifting surfaces.

The methods developed are capable of computing dynamic derivatives that are usually not computed or measured for in-plane and out-of-plane cases.

Computational comparison with data is fairly good for most cases. In general, the repeatability of dynamic derivative experimental values is much poorer than for static derivatives.

The current computer code, implementing the dynamic derivative models, requires about 330,000 octal storage locations for a 15-by-60 grid for full plane computations. Computational times for axial rate computations are about the same as for static computations. Plunging rate computations are about 50 percent longer.

## 6.0 REFERENCES

1. L. Devan, L. A. Mason, and F. G. Moore, *Aerodynamics of Tactical Weapons to Mach Number 8 and Angles-of-Attack 180 Degrees*, AIAA Paper 82-0250, AIAA 20th Aerospace Sciences Meeting, Orlando, FL, January 1982.
2. S. R. Vukelich and J. E. Jenkins, *Missile Datcom: Aerodynamic Prediction of Conventional Missiles Using Component Build-up Techniques*, AIAA Paper 84-0387, AIAA 22nd Aerospace Sciences Meeting, Reno, NV, January, 1984.
3. A. E. Magnus and M. A. Epton, *PAN AIR -- A Computer Program for Predicting Subsonic or Supersonic Linear Potential Flows About Arbitrary Configurations Using a Higher Order Panel Method, Vol. I -- Theory Document*, NASA CR-3251, 1980.

4. M. F. E. Dillenius and J. N. Nielsen, *Computer Programs for Calculating Pressure Distributions Including Vortex Effects on Supersonic Monoplane or Cruciform Wing-Body-Tail Combinations with Round or Elliptical Bodies*, NASA CR-3122, April 1979.
5. M. D. Van Dyke, *First- and Second-Order Theory of Supersonic Flow Past Bodies of Revolution*, Journal of the Aeronautical Sciences, March 1951.
6. L. Devan, *Conical, Noncircular, Second-Order, Potential Theory of Supersonic Flow*, AIAA Journal, Vol. 22, No. 5, May 1984.
7. L. Devan and L. A. Kania, *Nonaxisymmetric Body, Second-Order, Linear Supersonic Flow Prediction*, AIAA Paper 84-0313, AIAA 22<sup>nd</sup> Aerospace Sciences Meeting, Reno, NV January 1984.
8. L. Devan and L. A. Kania, *Nonaxisymmetric Discontinuous Body, Second-Order, Linear Supersonic Flow Prediction*, AIAA Paper 85-1810-CP, AIAA 12<sup>th</sup> Atmospheric Flight Mechanics Conference, Snowmass, CO, August 1985.
9. L. Devan, *Nonaxisymmetric Body, Supersonic, Aerodynamic Prediction*, AIAA Paper 87-2296-CP, AIAA 14<sup>th</sup> Atmospheric Flight Mechanics Conference, Monterey, CA, August 1987.
10. L. Devan, *Nonaxisymmetric Body, Supersonic, Aerodynamic Prediction*, NSWC TR 86-253, August 1987.
11. L. Devan, *NANC, Nonaxisymmetric Body, Supersonic Aerodynamic Prediction Code -- Program Description and Users Guide*, NSWC TR 87-167, October 1987.
12. L. Devan, *NANC, A Nonaxisymmetric Body, Supersonic Aeroprediction Code*, AIAA Paper 88-526, AIAA 26<sup>th</sup> Aerospace Sciences Meeting, Reno, NV, January 1988.
13. A. E. Gentry, D. N. Smyth, and W. R. Oliver, *The Mark IV Supersonic-Hypersonic Arbitrary-Body Program, Vol. I: Users Manual, Vol. II: Program Formulation, Vol. III: Program Listings*, AFFDL TR 73-159, November 1973.
14. J. W. Miles, *The Potential Theory of Unsteady Supersonic Flow*, Cambridge at the University Press, 1959.
15. P. Garcia-Fogeda, P. C. Chen, and D. D. Liu, *Unsteady Supersonic Flow Calculations for Wing-Body Combinations Using Harmonic Gradient Method*, AIAA Paper 88-0568, AIAA 26<sup>th</sup> Aerospace Sciences Meeting, Reno, NV, January 1988.

16. R. Courant and D. Hilbert, *Methods of Mathematical Physics*, Vol. II, Interscience Publishers, 1953, pp. 486-490.
17. R. W. MacCormack, *The Effect of Viscosity on Hypervelocity Impact Cratering*, AIAA Paper 69-354, Cincinnati, OH, April 1969.
18. C. P. Kentzer, *Discretization of Boundary Conditions in Moving Discontinuities*, Second International Conference on Numerical Methods in Fluid Dynamics, Berkeley, CA, September 1970.
19. L. E. Schmidt, *The Dynamic Properties of Pure Cones and Cone-Cylinders*, BRL Memorandum Report 759, January 1954.
20. R. H. Whyte, *SPIN-73, An Updated Version of the Spinner Computer Program*, Picatinny Arsenal TR-4558, November 1973.
21. J. D. Nicolaidis and L. C. MacAllister, *A Review of Aeroballistic Range Research on Winged and/or Finned Missiles*, Bureau of Ordnance, Ballistic Technical Note No. 5, 1955.
22. L. C. MacAllister, *The Aerodynamic Properties of a Simple Non-Rolling Finned Cone-Cylinder Configuration Between Mach Numbers 1.0 and 2.5*, BRL Report 934, May 1955.
23. M. Tobak, *Damping in Pitch of Low-Aspect Ratio Wings at Subsonic and Supersonic Speeds*, NACA RMA52L04A, April 1953.
24. R. Whyte, J. Burnett, and W. Hathaway, *Evaluation of the Computation of Pitch Damping Subroutine LMSC*, General Electric Armament Systems Department, Burlington, VT, November 1979.
25. P. Weinacht and W. Sturek, *Computation of the Roll Characteristics of Finned Projectiles*, BRL TR 2931, June 1988.
26. H. Fuchs, *Dynamic Derivatives of Missiles and Fighter-Type Configurations at High Angles of Attack*, Missile Aerodynamics Conference Honoring Dr. J. N. Nielsen, Monterey, CA, October 31-November 2, 1988.
27. R. G. Lacau, *Survey of Missile Aerodynamics*, Missile Aerodynamics Conference Honoring Dr. J. N. Nielsen, Monterey, CA, October 31-November 2, 1988.

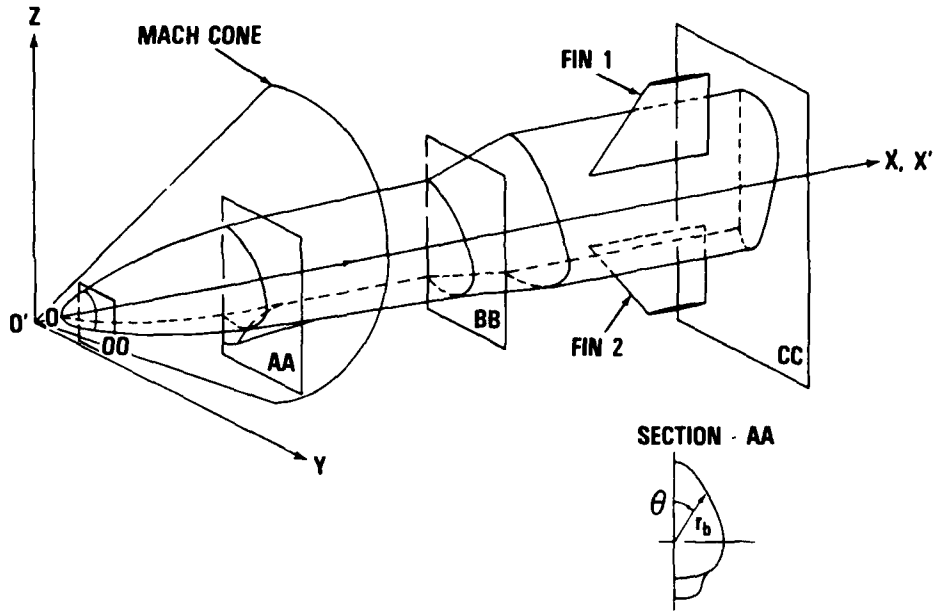


FIGURE 1. HALF BODY GEOMETRY

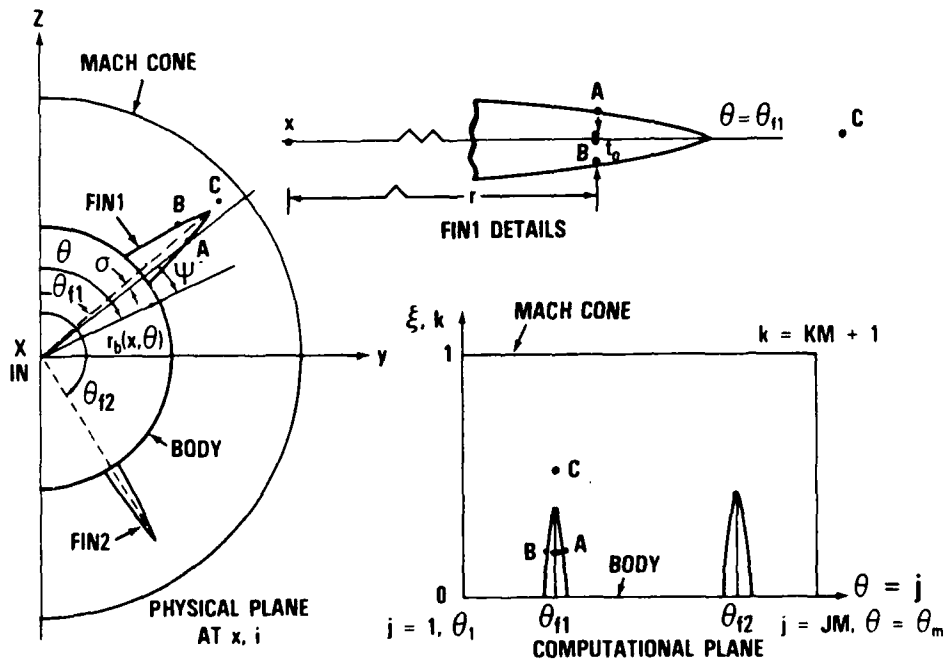


FIGURE 2. THIN FIN GEOMETRY

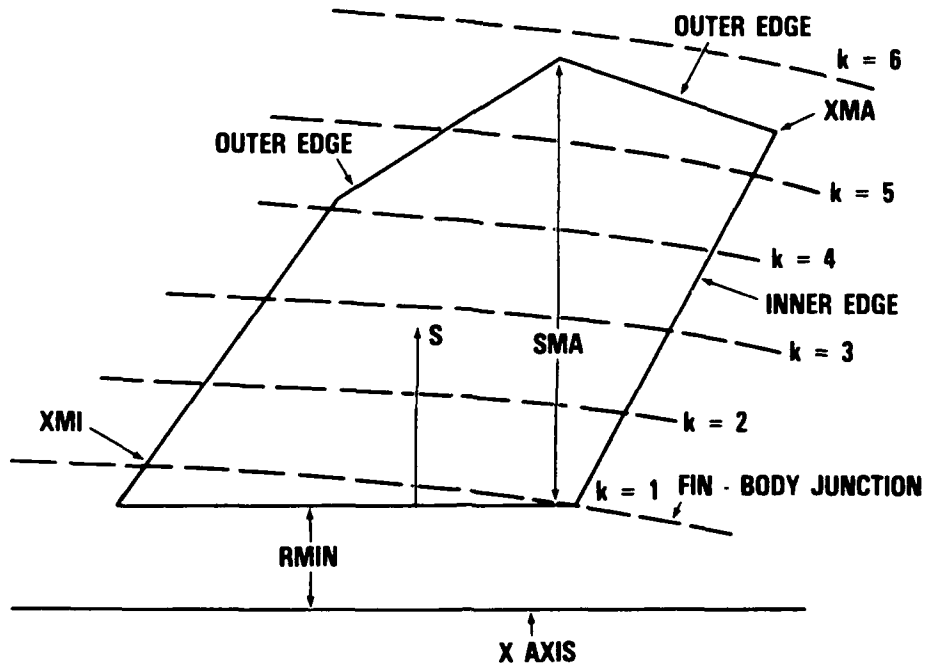


FIGURE 3. FIN PLANFORM GEOMETRY

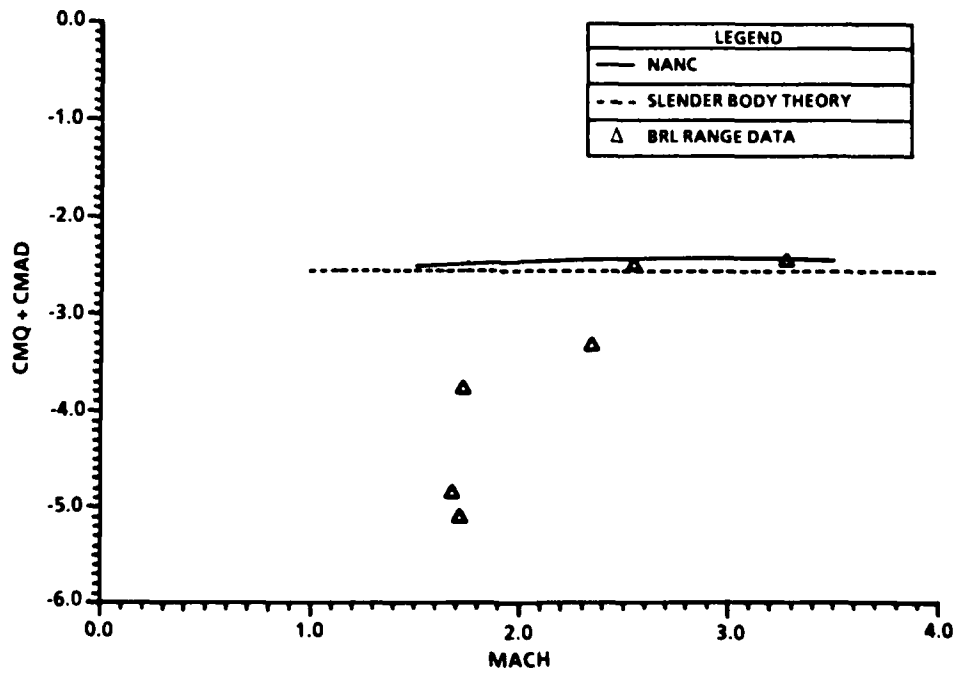


FIGURE 4.  $C_{mq} + C_{m\dot{\alpha}}$  COMPARISONS FOR A CIRCULAR CONE,  
 $L_N = 2.98$  CALIBERS,  $\alpha' = 2.18$  FROM NOSE

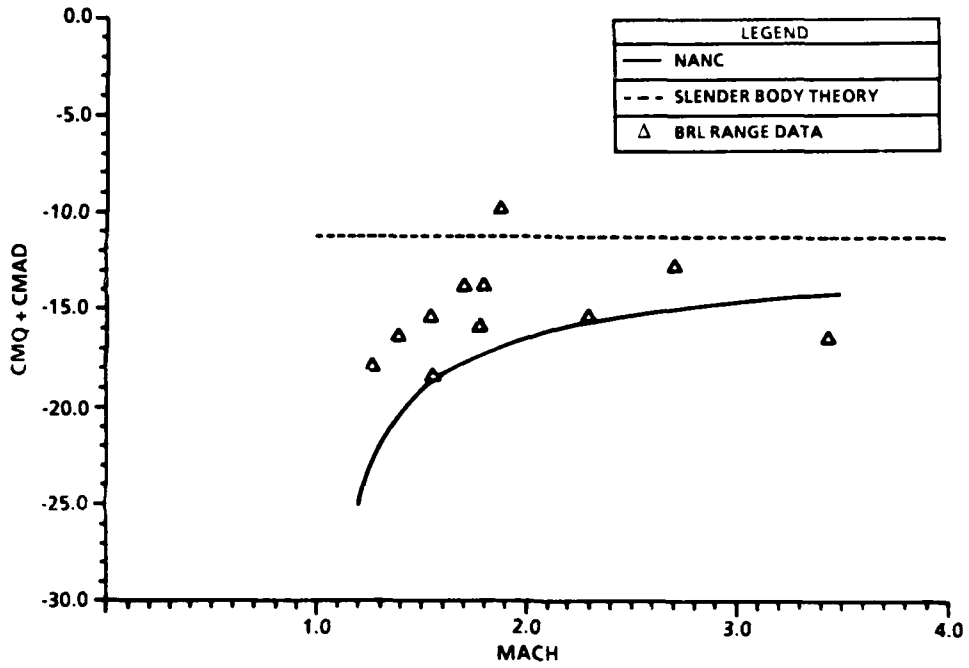


FIGURE 5.  $C_{mq}' + C_{m\dot{\alpha}}$  FOR A CONE-CYLINDER,  $L_N = 2.98$  CALIBERS,  $L = 5.12$  CALIBERS,  $x' = 3.44$  CALIBERS FROM NOSE

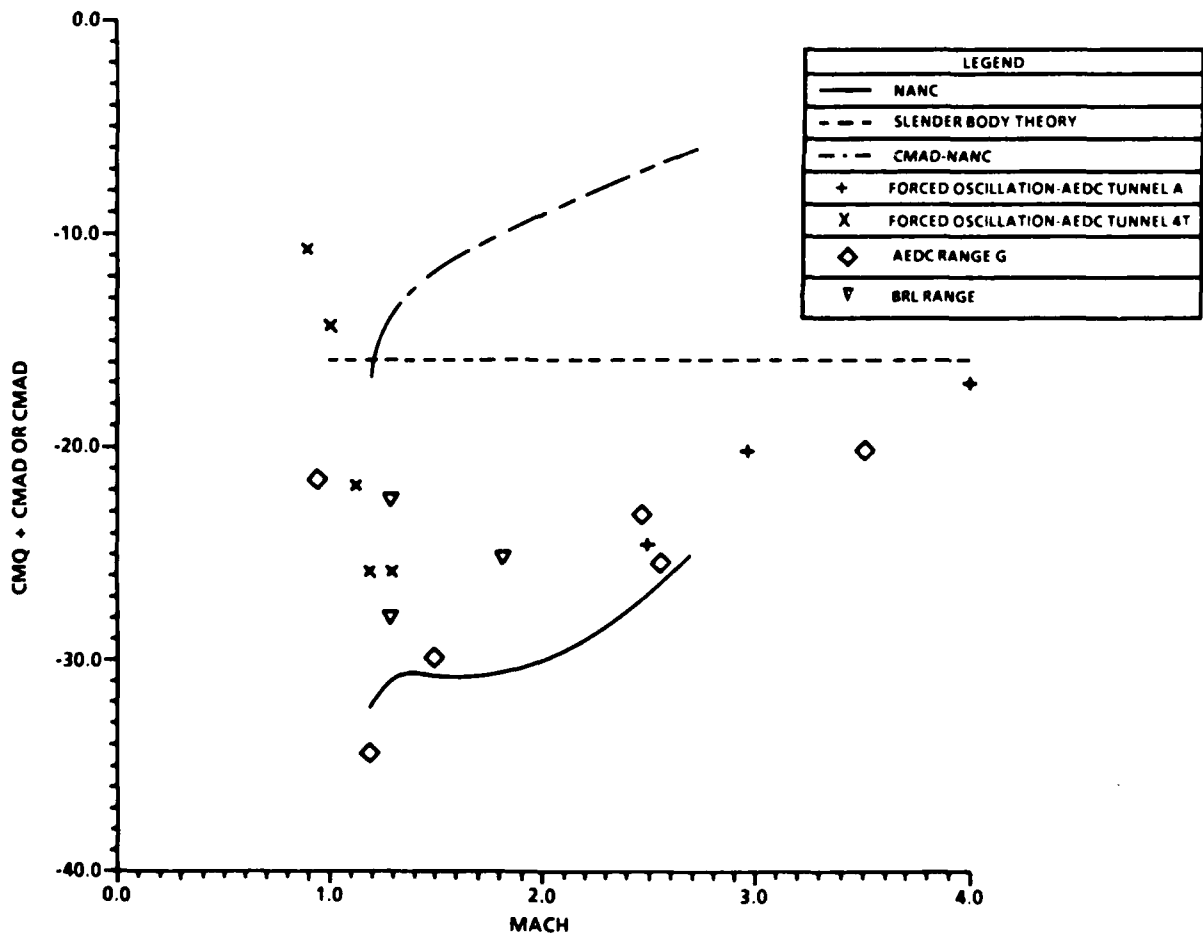


FIGURE 6.  $C_{mq}' + C_{m\dot{\alpha}}$  COMPARISON FOR THE ARMY-NAVY SPINNER,  $L_N = 2.0$  CALIBERS,  $L = 5.0$  CALIBERS,  $x' = 3.0$  CALIBERS FROM NOSE

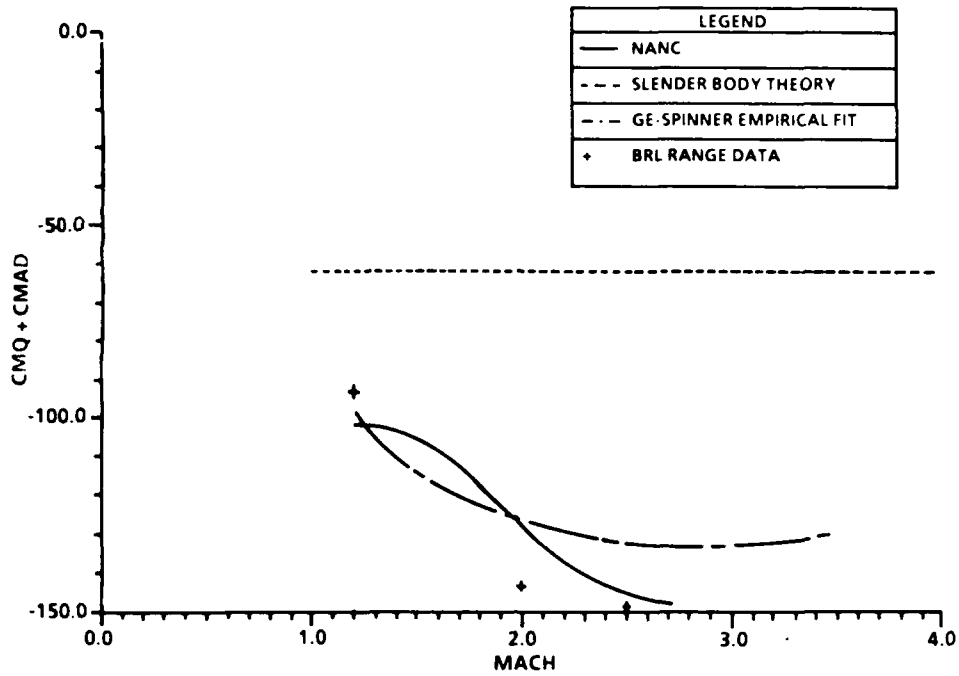


FIGURE 7.  $C_{mq}' + C_{m\dot{\alpha}}$  FOR THE ARMY-NAVY SPINNER,  $L_N = 2.0$  CALIBERS,  $L = 9.0$  CALIBERS,  $x' = 5.06$  CALIBERS FROM NOSE

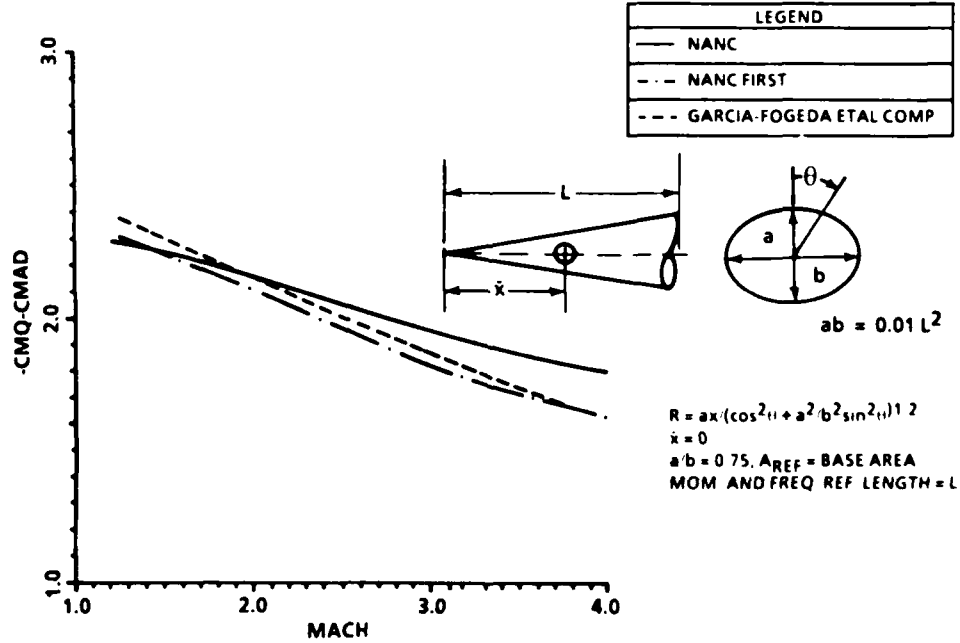


FIGURE 8.  $C_{Nq}' + C_{N\dot{\alpha}}$  COMPARISON FOR AN ELLIPTIC CONE

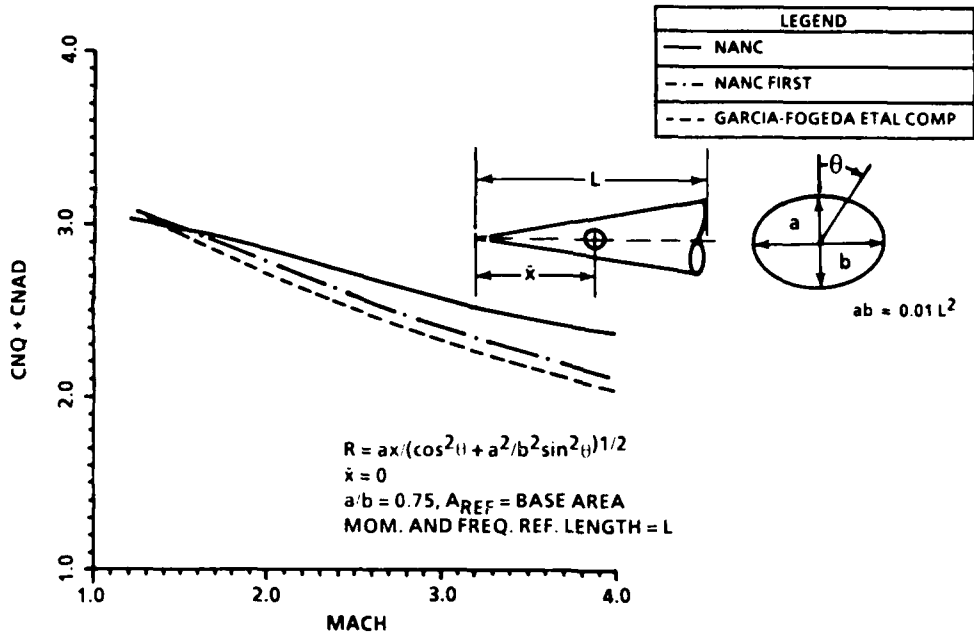


FIGURE 9.  $C_{mq}' + C_{m\dot{\alpha}}$  COMPARISON FOR AN ELLIPTIC CONE

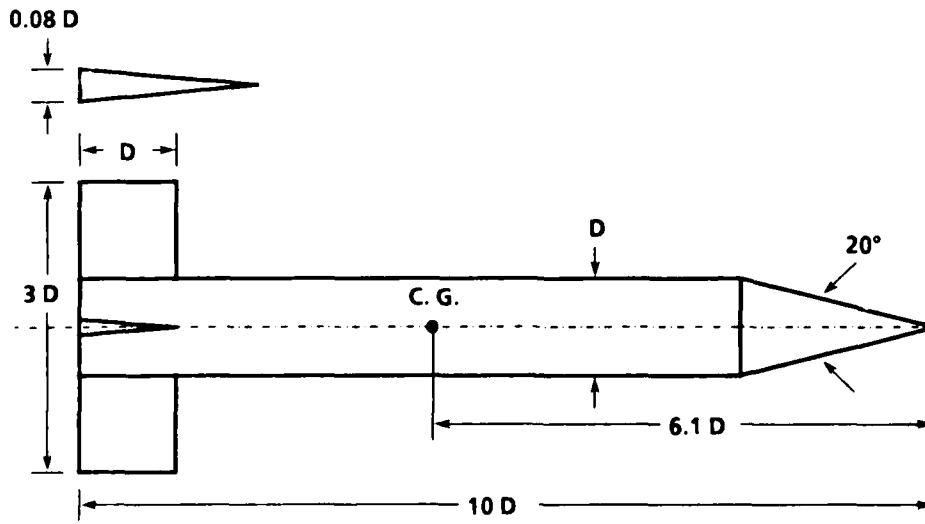


FIGURE 10. BASIC FINNER CONFIGURATION

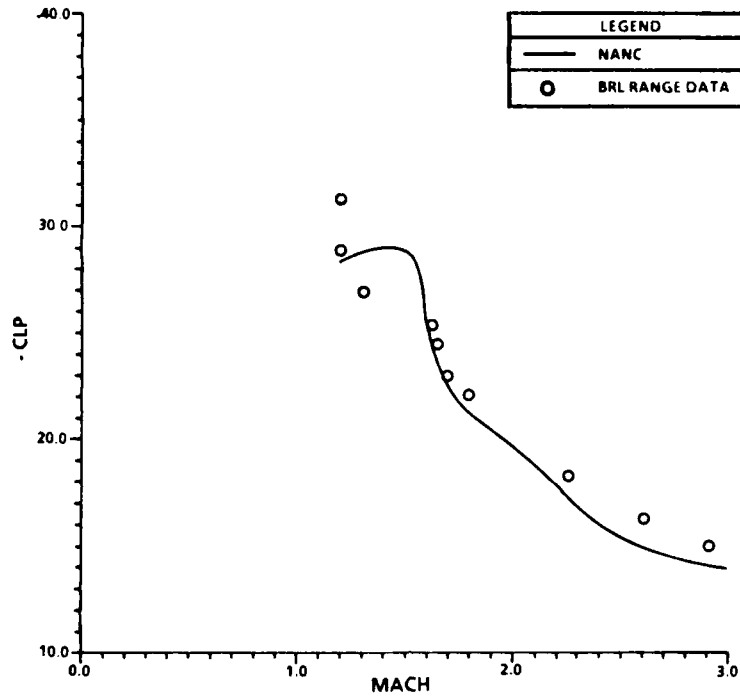


FIGURE 11. BASIC FINNER  $C_{l_p}'$  COMPARISON

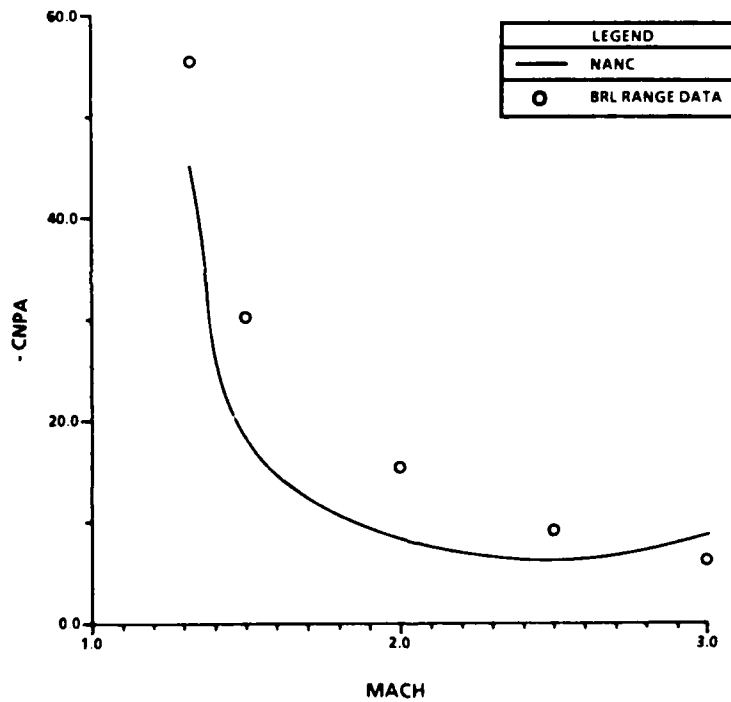


FIGURE 12.  $C_{np}'$ , MAGNUS DERIVATIVE FOR THE BASIC FINNER

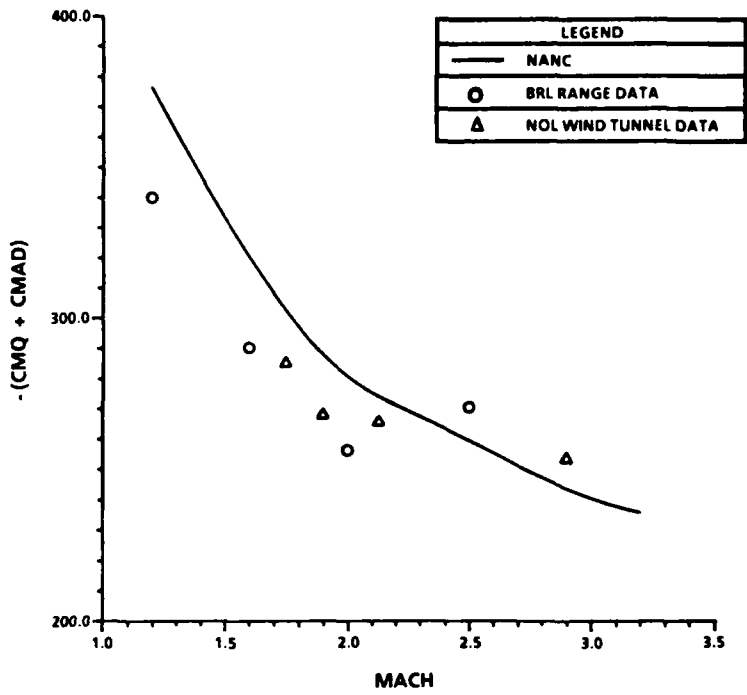
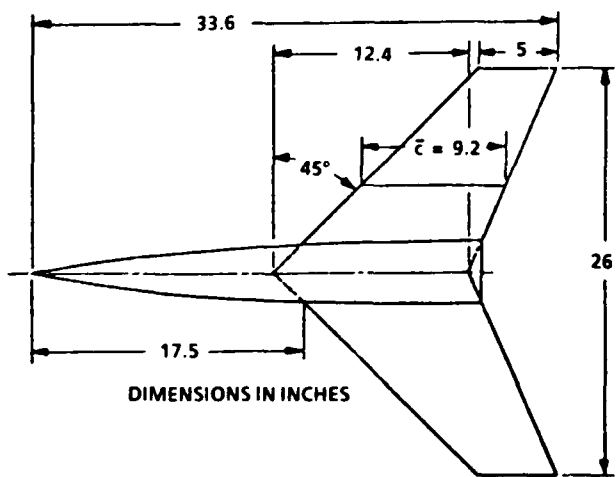
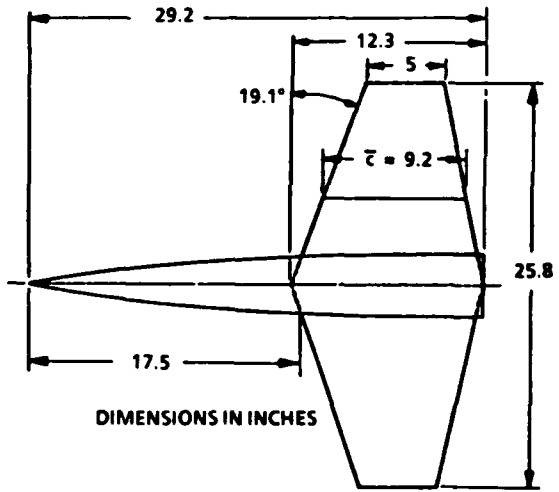


FIGURE 13. TOTAL PITCH DAMPING COMPARISON FOR THE BASIC FINNER



(a) A = 3 SWEEP WING (3% BICONVEX CIRCULAR-ARC SECTIONS)



(b) A = 3 UNSWEEP WING (3% BICONVEX CIRCULAR-ARC SECTIONS)

FIGURE 14. ASPECT RATIO = 3 CONFIGURATIONS

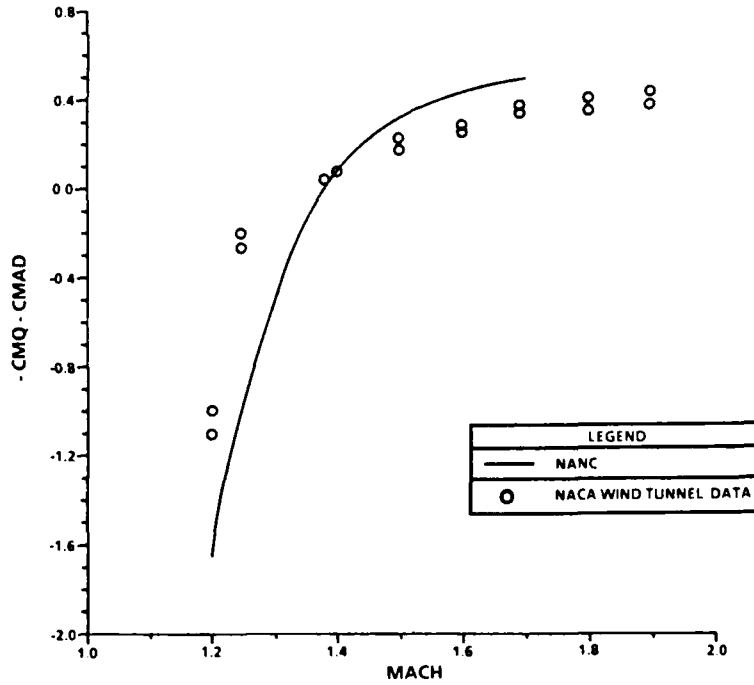


FIGURE 15. PITCH DAMPING COMPARISON FOR AN AR = 3 WING-BODY CONFIGURATION

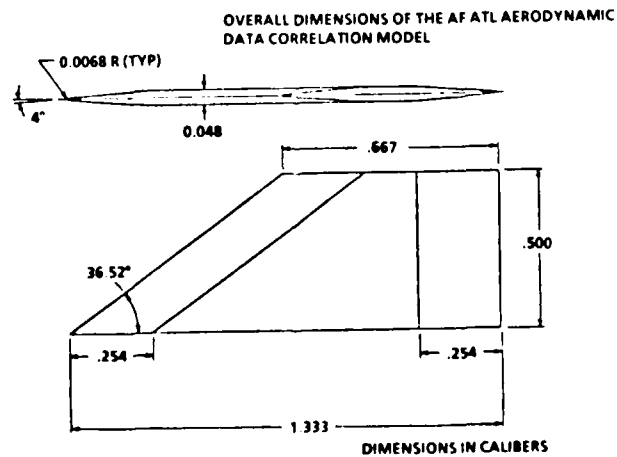
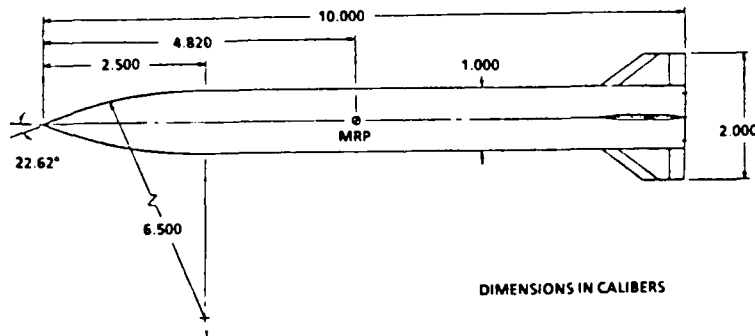


FIGURE 16. AIR SLEW DEMONSTRATOR VEHICLE

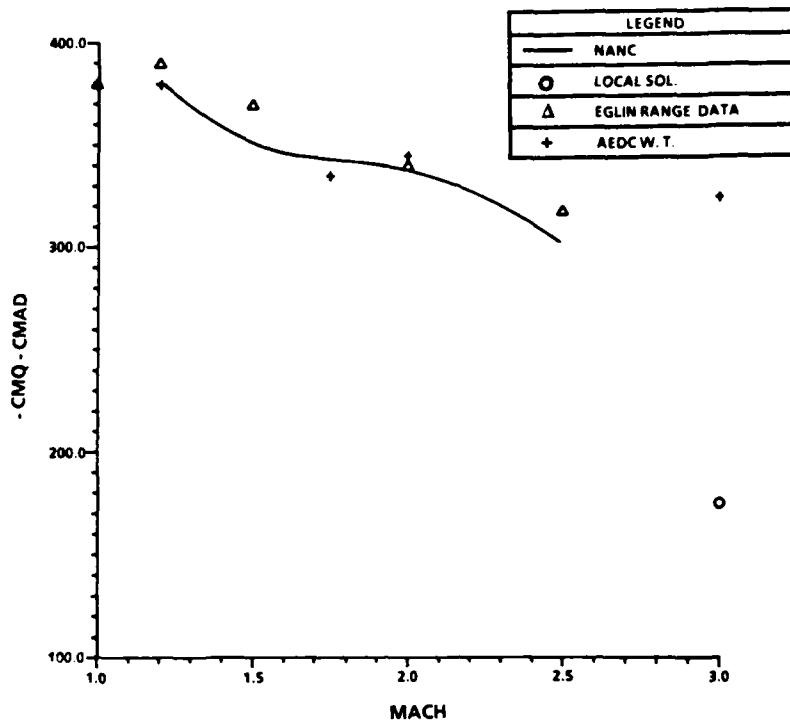


FIGURE 17. PITCH DAMPING COMPARISON FOR THE AIR SLEW DEMONSTRATOR VEHICLE

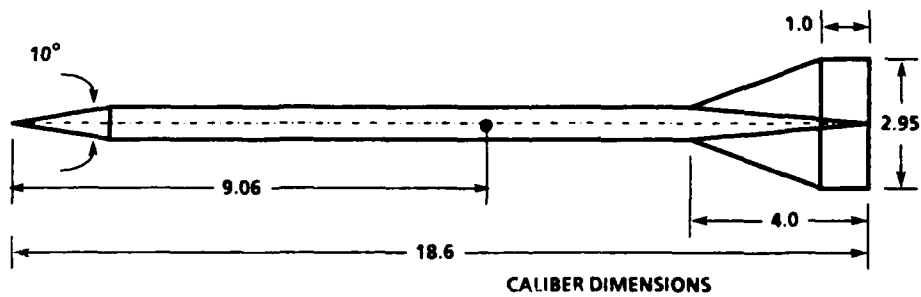


FIGURE 18. XM-144 CONFIGURATION

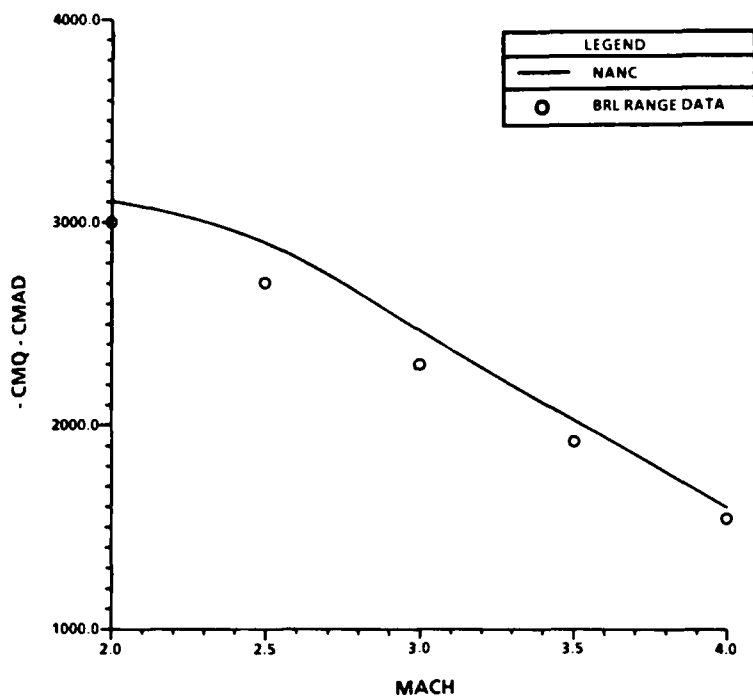
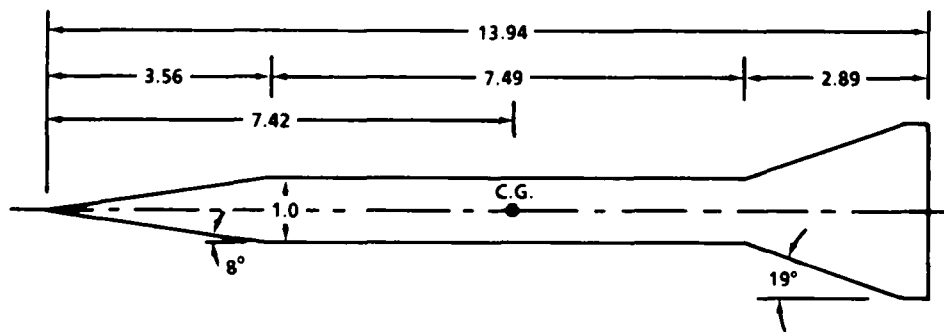


FIGURE 19. TOTAL PITCH DAMPING FOR THE XM-144



ALL DIMENSIONS IN CALIBERS (ONE CALIBER = 35.2 mm)

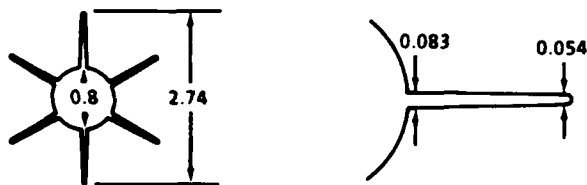


FIGURE 20. BRL M735 CONFIGURATION

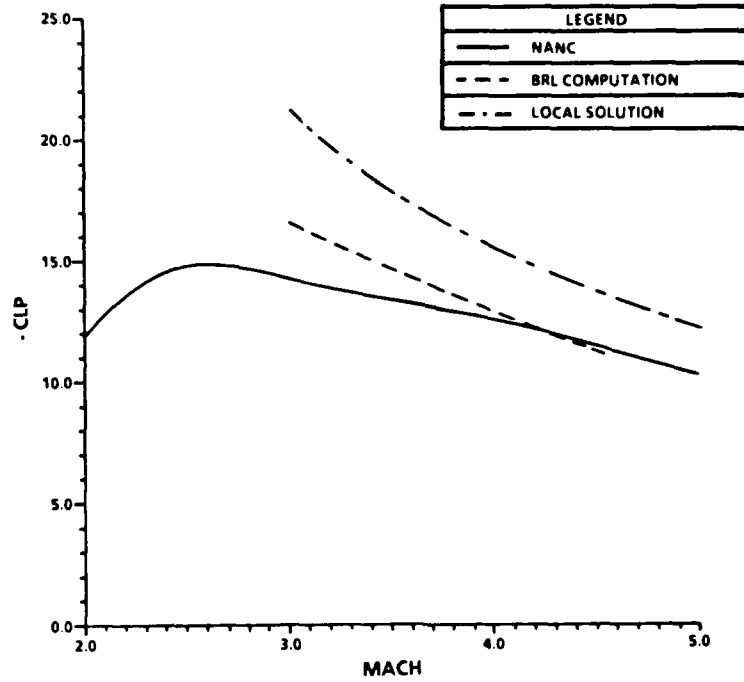


FIGURE 21. ROLL DAMPING COMPARISON COMPUTATIONS FOR THE M735 PROJECTILE

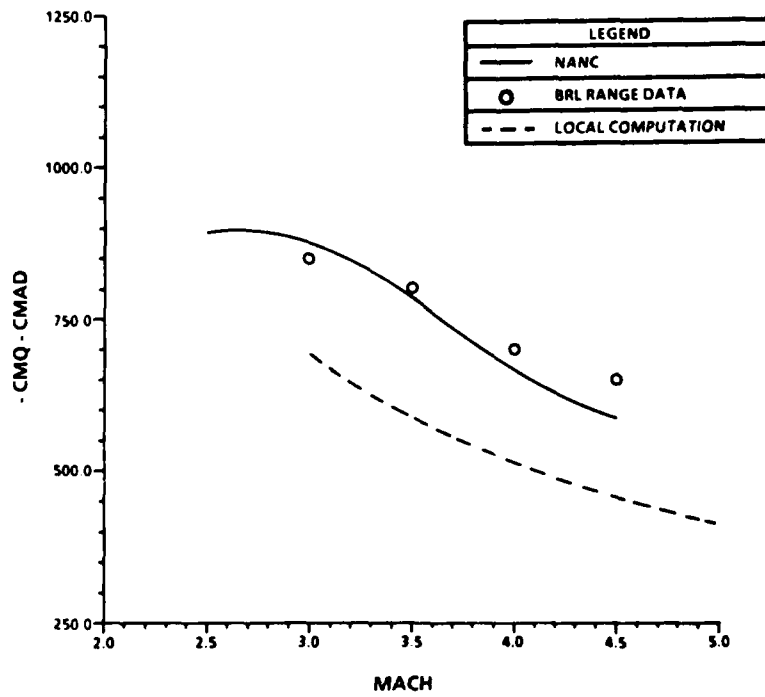


FIGURE 22. TOTAL PITCH DAMPING COMPARISON FOR THE M735 PROJECTILE

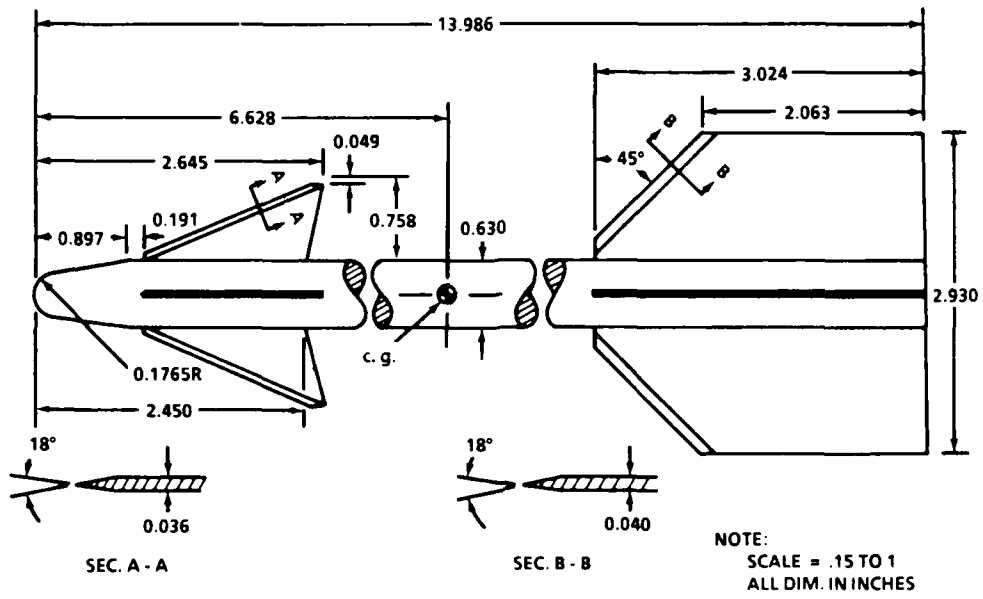


FIGURE 23. SIDEWINDER GEOMETRY

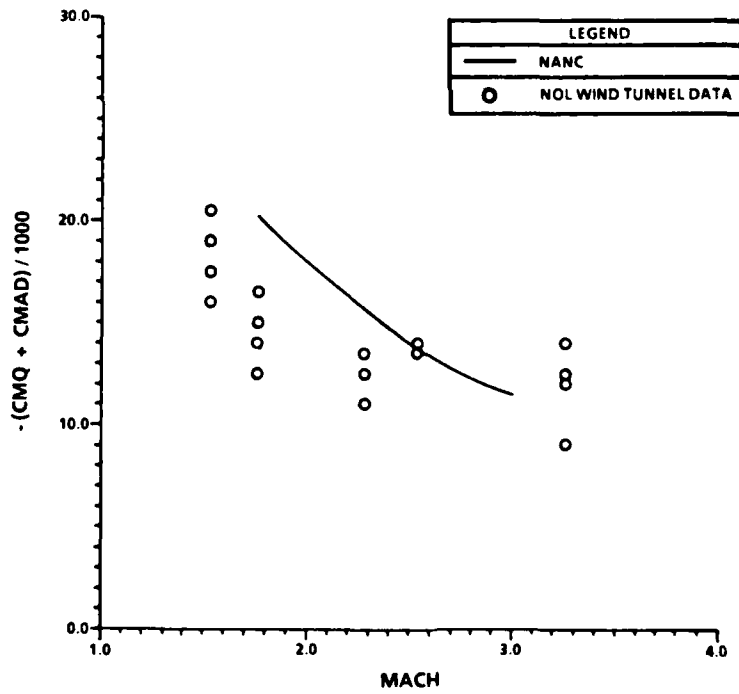


FIGURE 24. TOTAL PITCH DAMPING COMPARISON FOR THE SIDEWINDER

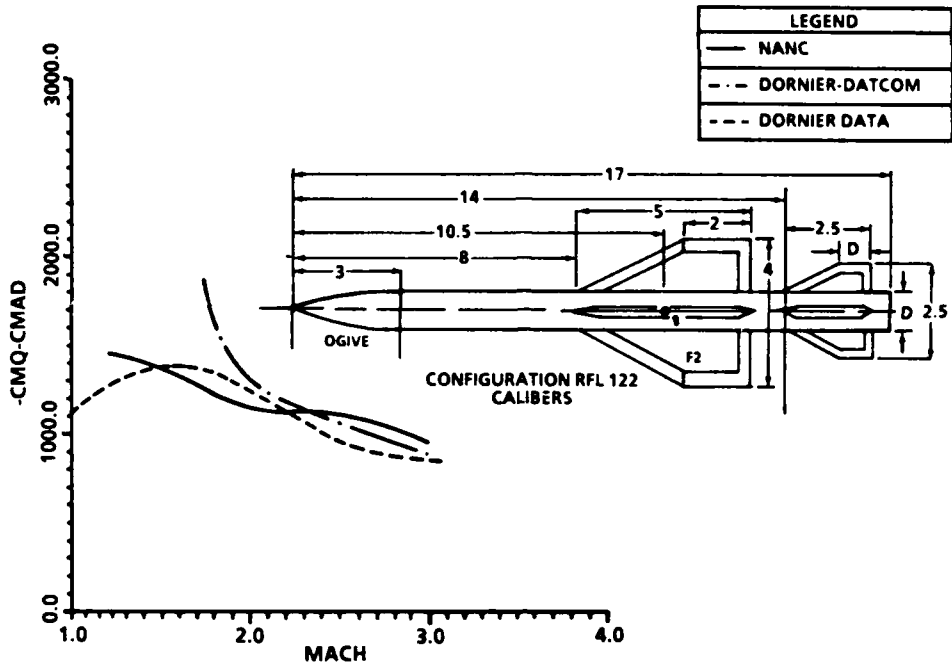


FIGURE 25. TOTAL PITCH DAMPING COMPARISON FOR THE RFL 122

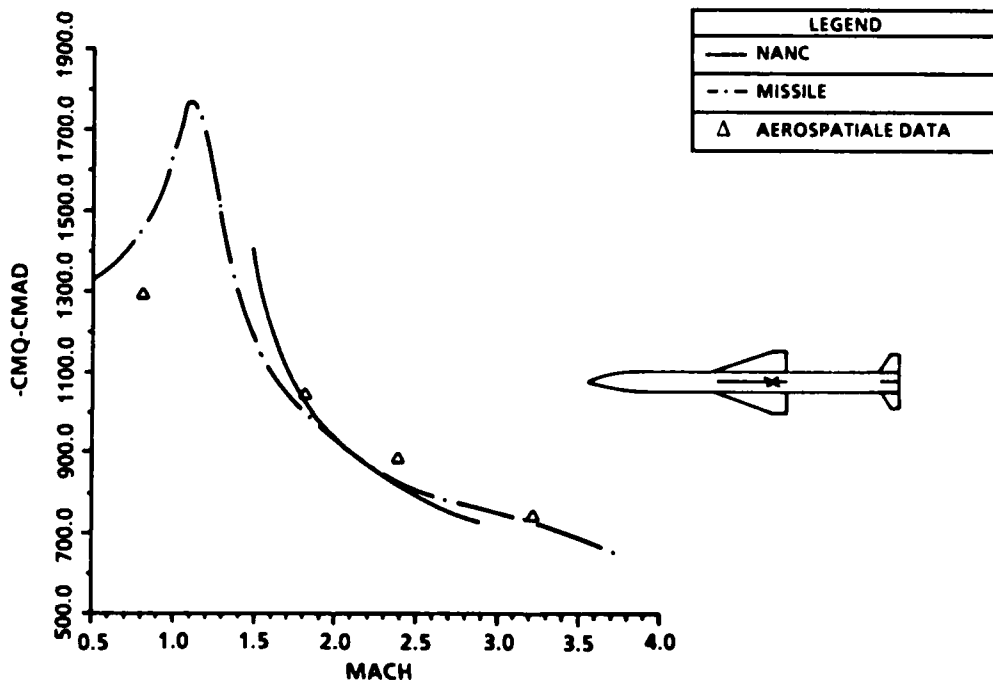


FIGURE 26. TOTAL PITCH DAMPING COMPARISON FOR AN AEROSPATIALE MISSILE CONFIGURATION

**APPENDIX  
NOMENCLATURE**

## NOMENCLATURE

$a$	Dimensionless speed of sound
$a_\infty$	Reference speed of sound = free-stream value
$C_i$	General force or moment coefficient
$C_p$	Pressure coefficient
$i$	Grid index for a constant $x$ plane
$i'$	Unit vector in $x$ direction
$j$	Grid index for constant $\theta$ plane
$j'$	Unit vector in $y$ or $r$ direction
$k$	Grid index for constant $\xi$ plane
$k'$	Unit vector in $z$ or $\theta$ direction
LM	Aerodynamic symmetry mode
$M_i$	Moment or force
$M_\infty$	Free-stream Mach number
$n$	Unit normal vector from a solid surface
$p'$	Rotational rate about the $x$ axis
	(NOTE: All $q$ velocities are nondimensional)
$q$	Perturbation velocity vector
$q'$	Rotation rate about $y$ axis
$q_a$	Velocity vector associated with $\phi_a$ potential
$q_{ax}$	Velocity vector at $t = 0$ due to plunging acceleration

$q_b$	Velocity vector associated with $\phi_b$ potential
$q_{0\infty}$	Equivalent free-stream velocity vector relative to body axes
$q_r$	$Q - V$ , relative velocity
$q_x$	Equivalent free-stream velocity vector relative to body coordinates at $t = 0$
$\dot{q}_x$	Free-stream acceleration relative to body axes (dimensionless)
$q'_x$	Equals $q_{0\infty} - i'$
$q_1$	First-order velocity vector, steady part
$q'_1$	Total first-order velocity vector
$q_2$	Second-order velocity vector
$q_{1c}$	First-order crossflow vector
$Q$	Total velocity vector of fluid in body axis coordinates relative to gas at rest
$Q_D$	$1/2 \rho_x V^2$ , dynamic pressure
$Q_{Te}$	Total first- or second-order velocity vector, $t = 0$
$r$	Radial coordinate
$r'$	Rotation rate for z direction
$r_b$	Body radius
$r_o$	Body radius to outer fin edge
$S_R$	Reference area
$t$	Time
$t_x$	Fin slope in x direction
$u$	x component of perturbation velocity
$\dot{u}_0$	x component of c. g. acceleration

$u'_1$	x component of $q'_1$
$v$	r component of perturbation velocity
$\dot{v}_0$	y component of c. g. acceleration
$V$	Equals $-q_{0,x}$ , velocity relative to gas at rest in body axis coordinates
$V_\infty$	Magnitude of velocity vector of c. g. at $t = 0$
$w$	$\theta$ component of perturbation velocity
$\dot{w}_0$	z component of c. g. acceleration
$x$	Cartesian coordinate from nose -- zero incidence direction
$x'$	Moment center distance from nose
$x_R$	Reference length
$x_D$	Reference length associated with reduced frequency
$y$	Cartesian coordinate perpendicular to vertical body symmetry plane (to the right looking downstream)
$z$	Cartesian coordinate perpendicular to x, y plane (up, looking downstream)
$\alpha$	Angle of attack
$\beta$	Equals $\sqrt{M_\infty^2 - 1}$
$\beta'$	Angle of side slip
$\gamma$	Specific heat ratio
$\epsilon_0$	Equals $(\partial r_b / \partial \theta) / r_b$
$\zeta$	Equals $\zeta(\xi)$ , clustering transformation in $\xi$ direction
$\theta$	Cylindrical coordinate angle from leeside plane
$\xi$	Equals $(r - r_b) / (x / \beta - r_b)$ , shearing transformation
$\rho$	Density

$\rho_\infty$	Free-stream density
$\phi$	Disturbance potential
$\phi_1$	First-order disturbance potential for $\dot{q}_x = 0$
$\phi_1'$	Equals $\phi_1 + (M_\infty/\beta^2)\phi_a + V_\infty[t - xM_\infty^2/(\beta^2V_\infty)]\phi_b$  (Total first-order disturbance potential $\phi_a$ and $\phi_b$ are equivalent static problem potentials.)
$\phi_2$	Second-order disturbance potential
$\Phi$	Equals $\Phi(\theta)$ -- clustering transformation in $\theta$ direction
$x$	Absolute temperature ratio
$\omega_i$	General term in computing reduced frequency

## DISTRIBUTION

	<u>Copies</u>		<u>Copies</u>
Commander		Commander	
Naval Sea Systems Command		Naval Development Center	
Attn: SEA-62G2 (Mr. L. Pasiuk)	1	Attn: Mr. S. Greenhalgh	1
Technical Library	1	Mr. W. Tseng	1
Washington, DC 20362-5101		Dr. A. Cenko	1
		Technical Library	1
Commander		Warminster, PA 18974	
Naval Air Systems Command		Superintendent	
Attn: AIR-93D (Dr. G. Heiche)	1	U. S. Naval Academy	
AIR-932J (Mr. D. Hutchins)	1	Attn: Head, Weapons Dept.	1
Technical Library	1	Head, Science Dept.	1
Washington, DC 20361-0001		Technical Library	1
Commander		Annapolis, MD 21402	
Naval Weapons Center		Superintendent	
Attn: Technical Library	1	U. S. Naval Postgraduate School	
Mr. C. S. Porter	1	Attn: Prof. T. Sarpkaya	1
Dr. R. G. Burman	1	Dr. R. Howard	1
Mr. R. E. Smith	1	Dr. D. Salinas	1
Mr. L. W. Strutz	1	Technical Library	1
China Lake, CA 93555-6001		Monterey, CA 95076	
Commander		Officer in Charge	
Naval Ship Research and Development Center		Naval Intelligence Support Center	
Attn: Dr. J. Schott	1	Attn: Dr. M. Krumins	1
Technical Library	1	Technical Library	1
Washington, DC 20007		4301 Suitland Road	
Chief of Naval Research		Washington, DC 20390	
Attn: Mr. D. Siegel (ONT)	1	Commanding Officer	
Dr. R. Whitehead	1	Naval Ordnance Station	
Dr. S. Lykoudis	1	Attn: Technical Library	1
Dr. T. C. Tai	1	Indian Head, MD 20640	
Technical Library	1		
800 N. Quincy Street			
Arlington, VA 22217			

## DISTRIBUTION (CONTINUED)

	<u>Copies</u>		<u>Copies</u>
Commanding Officer Naval Weapons Support Center Attn: Code 5062 (Mr. D. Jensen) Crane, IN 47522	1	Arnold Engineering Develop- ment Center USAF Attn: Dr. D. Daniel Technical Library Tullahoma, TN 37389	1 1
Defense Intelligence Agency Attn: DIAC/DT-4A (Mr. P. Murad) Washington, DC 20546	1	Commanding Officer Air Force Armament Labora- tory (AFATL) Attn: Dr. D. Belk Mr. C. Cottrell Mr. S. Korn Dr. L. E. Lijewski Elgin AFB, FL 32542	1 1 1 1
Commanding General Ballistic Research Laboratory Attn: Dr. C. H. Murphy Dr. R. Sedney Dr. W. Sturek Mr. C. Nietubicz Dr. A. Mikhail Technical Library Aberdeen, MD 21005	1 1 1 1 1 1	Commanding Officer Air Force Wright Aeronautical Laboratories (AFSC) Attn: Dr. V. Dahlem Mr. M. Pinney Dr. G. Kurylowich Mr. D. Shereda Mr. J. Jenkins Wright-Patterson AFB, OH 45433	1 1 1 1 1
Commander U. S. Army ARDEC Attn: Mr. R. W. Kline Mr. J. Grau Technical Library Picatinny Arsenal, NJ 07806	1 1 1 1	Commanding Officer HQ/FTD/SDDV (72651) Attn: Mr. R. D. Samuels Wright-Patterson AFB, OH 45433	1
Commanding General U. S. Army Missile R&D Command DROMI-TDK Redstone Arsenal Attn: Mr. Billy J. Walker Dr. C. D. Mikkelsen Technical Library Huntsville, AL 35809	1 1 1	USAF Academy Attn: Technical Library Colorado Springs, CO 80912	1
Commanding Officer Harry Diamond Laboratories Attn: Technical Library Adelphi, MD 20783	1	Advanced Research Projects Agency Department of Defense Attn: Technical Library Washington, DC 20305	1

## DISTRIBUTION (CONTINUED)

	<u>Copies</u>		<u>Copies</u>
NASA Attn: Technical Library Washington, DC 20546	1	The University of Tennessee Space Institute Attn: Prof. J. M. Wu Technical Library Tullahoma, TN 37388	1 1
NASA Ames Research Center Attn: Dr. G. Chapman Dr. J. Nielsen Technical Library Moffett Field, CA 94035	1 1 1	University of Notre Dame Department of Aerospace and Mechanical Engineering Attn: Dr. R. Nelson Technical Library Notre Dame, IN 46556	1 1
NASA Langley Research Center Attn: Mr. J. South Mr. C. M. Jackson, Jr. Mr. W. C. Sawyer Mr. J. M. Allen Technical Library Hampton, VA 23365	1 1 1 1 1	Purdue University School of Engineering and Technology Attn: Prof. A. Ecer Technical Library P. O. Box 647 1201 E. 38th Street Indianapolis, IN 46223	1 1
Library of Congress Attn: Gift and Exchange Division Washington, DC 20540	4	Stanford University Department of Aeronautics and Astronautics Attn: Prof. M. D. Van Dyke Technical Library Stanford, CA 94305	1 1
Virginia P.I.S. University Department of Aerospace and Ocean Engineering Attn: Prof. J. A. Schetz Prof. B. Grossman Technical Library Blacksburg, VA 24060	1 1 1	University of Texas Aerospace Engineering and Engi- neering Mechanics Department Attn: Prof. J. J. Bertin Technical Library Austin, TX 78712	1 1
North Carolina State University Department of Mechanical and Aerospace Engineering Attn: Prof. F. R. DeJarnette Prof. H. A. Hassan Technical Library Box 5246 Raleigh, NC 27607	1 1 1		

## DISTRIBUTION (CONTINUED)

	<u>Copies</u>		<u>Copies</u>
The Johns Hopkins University Applied Physics Laboratory Attn: Mr. E. T. Marley	1	Lockheed Missiles and Space Company, Inc. Attn: Mr. T. Lundy	1
Mr. E. Lucero	1	Huntsville, AL 35807	
Mr. L. E. Tisserand	1	Sverdrup Technology Attn: Mr. M. S. Miller	1
Mr. R. E. Lee	1	P. O. Box 1935 Elgin AFB, FL 32542	
Johns Hopkins Road Laurel, MD 20810		Nielsen Engineering and Research, Inc. Attn: Dr. M. Mendenhall	1
Raytheon Missile Systems Attn: Mr. R. Sterchele	1	Dr. M. F. E. Dillenius	1
Dr. D. P. Forsmo	1	510 Clyde Avenue Mountain View, CA 95043	
Dr. H. T. Flomenhoft	1	General Electric Company Armament Systems Department Attn: Mr. R. Whyte	1
P. O. Box 1201 Tewksbury, MA 01876-0901		Burlington, VT 05401	
McDonnell-Douglas Astronautics Company (West) Attn: Dr. J. Xerikos	1	CALSPAN PWT-4T MS-600 Attn: Dr. W. B. Baker, Jr.	1
5301 Bolsa Avenue Huntington Beach, CA 92647		Mr. W. A. Crosby	1
McDonnell-Douglas Astronautics Company (East) Attn: Mr. J. Williams	1	Arnold AFS, TN 37389	
Dr. R. Krieger	1	Ling-Temco-Vought Attn: Mr. F. Prillman	1
Mr. S. Vukelich	1	Dr. W. B. Brooks	1
Box 516 St. Louis, MO 61366		Mr. R. Stancil	1
Lockheed Missiles and Space Company, Inc. Attn: Dr. L. E. Ericsson	1	P. O. Box 5907 Dallas, TX 75222	
Mr. P. Reding	1		
Sunnyvale, CA 94086			

## DISTRIBUTION (CONTINUED)

	<u>Copies</u>		<u>Copies</u>
Hughes Aircraft Corporation Attn: Mr. R. Reed Mr. H. August Canoga Park, CA 91304	1 1	VRA, Inc. Attn: Dr. C. H. Lewis P. O. Box 50 Blacksburg, VA 24060	1
Northrup Corporation Aircraft Group Attn: Dr. J. Sun 1515 Rancho Conejo Blvd. Newbury Park, CA 91320	1	Integrated Systems, Inc. Attn: Mr. M. M. Briggs 151 University Avenue Palo Alto, CA 94301	1
Sandia National Laboratories Attn: Dr. W. Oberkampf Mr. W. Rutledge Albuquerque, NM 87115	1 1	DEI Tech., Inc. Attn: Mr. K. Walkley 11838 Bunker Blvd., Suite 500 Newport News, VA 23606	1
Martin Marietta Aerospace Co. Attn: Mr. L. A. Kania Mr. J. Donahue P. O. Box 5837 Orlando, FL 32805	1 1	Grumman Aerospace Corporation Research and Development Center M. S. A 08-35 Attn: Dr. M. J. Siclari Bethpage, NY 11714	1
Motorola, Inc. Missile System Operations Attn: Mr. G. H. Rapp P. O. Box 1417 Scottsdale, AZ 85252	1	Olin Corporation Attn: Mr. L. A. Mason P. O. Box G Marion, IL 62959	1
TRW Space and Technology Group Attn: Dr. T. Shivananda One Space Park Redondo Beach, CA 90278	1	United Technologies Norden Systems Attn: Dr. G. Ramanathan Mr. M. Fink M. S. K041 Norwalk, CT 06856	1 1
TRW Electronics and Defense Sector Attn: Dr. T. Lin Building 527 P. O. Box 1310 San Bernadino, CA 92402	1	Aerojet Tactical Systems Co. Attn: Mr. D. O. Matejka Sacramento, CA 98513	1

## DISTRIBUTION (CONTINUED)

	<u>Copies</u>		<u>Copies</u>
General Dynamics Convair Division Attn: Mr. K. Hively Mr. D. Brower P. O. Box 85357 San Diego, CA 92138	1 1	Teledyne Ryan Aeronautical Attn: Mr. J. C. Grams 2701 Harbor Drive San Diego, CA 92138	1
AVCO Systems Division Attn: Mr. E. Lawlor 201 Lowell Street Wilmington, MA 01887	1	Goodyear Aerospace Corporation Attn: Mr. S. Black 1210 Massilan Road Akron, OH 44315	1
Aerojet Electro Systems Co. Attn: Dr. Y. C. Shen P. O. Box 296-III Azusa, CA 91702	1	Texas Instruments, Inc. Attn: Mr. D. Vosburgh M. S. 3405 P. O. Box 405 Louisville, TX 75067	1
North American Aircraft Operations Rockwell International Attn: Mr. R. Cavage Dr. E. Bonner P. O. Box 92098 Los Angeles, CA 90009	1 1	DYNA East Corporation Attn: Mr. W. J. Clark 3132 Market Street Philadelphia, PA 19104	1
PRC Kentron Attn: Dr. M. Hemsch 3221 N. Armisted Avenue Hampton, VA 23666	1	<u>Internal Distribution:</u> E E211 (M. Green) E231 E31 (GIDEP) F G G06 G10 G13 G20 G205 G21 G22	1 1 10 1 1 1 1 1 1 1 1 1 1 1
Tracor Aerospace, Inc. Attn: Mr. W. Estes MIS 6-5 6500 Tracor Lane Austin, TX 78721	1		

## DISTRIBUTION (CONTINUED)

	<u>Copies</u>
<u>Internal Distribution (Cont'd):</u>	
G23	1
G23 (Devan)	20
G23 (Hardy)	1
G30	1
G33	1
G40	1
G42 (Graff)	1
H	1
K	1
K20	1
K204	1
K22	1
K24	1
N	1
N40	1
R	1
R44 (Wardlaw, Priolo)	2
U	1